Is the diatom sex clock a clock?

Thomas Fuhrmann-Lieker*, Nico Kubetschek, Jonas Ziebarth

Physical Chemistry of Nanomaterials, Institute of Chemistry and Center for Interdisciplinary Nanostructure Science and Technology, Faculty of Mathematics and Natural Sciences, University of Kassel, D-34109 Kassel, Germany

Roland Klassen

Microbiology, Institute of Biology and Center for Interdisciplinary Nanostructure Science and Technology, Faculty of Mathematics and Natural Sciences, University of Kassel, D-34109 Kassel, Germany

Werner Seiler

Algorithmic Algebra and Discrete Mathematics, Institute of Mathematics, Faculty of Mathematics and Natural Sciences, University of Kassel, D-34109 Kassel, Germany

*th.fuhrmann@uni-kassel.de

Abstract (<200 words)

The unique life cycle of diatoms with continuous decreasing and restoration of the cell size leads to periodic fluctuations in cell size distribution and has been regarded as a multi-annual clock. For understanding the long-term behaviour of a population analytically, generic mathematical models are investigated algebraically and numerically for their capability of describing periodic oscillations. Whereas the generally accepted simple concepts for the proliferation dynamics do not sustain oscillating behaviour due to broadening of the size distribution, simulations show that a proposed limited lifetime of a newly synthesized cell wall slows down the relaxation towards a time-invariant equilibrium state to the order of hundred thousand generations. In combination with seasonal perturbation events, the proliferation scheme with limited lifetime is able to explain long-lasting rhythms that are characteristic for diatom population dynamics. The life cycle thus resembles a pendulum clock that has to be wound up from time to time by seasonal perturbations rather than an oscillator represented by a limit cycle.

Keywords

Diatoms, oscillations, clocks, discrete models, matrix models

1. Introduction

Phytoplankton plays an enormous role in the sequestration of carbon dioxide from the atmosphere.[1,2] From the estimated 60 gigatons of carbon fixation per year in the oceans, 26 gigatons are attributed to diatoms, both values being maximum estimates.[3] Additional contributions come from freshwater in which diatoms are also abundant, leading to a total share of 20-25% of primary production worldwide. However, the productivity is subjected to periodic fluctuations in the form of so-called algal blooms.[4,5] Whereas a major part of these fluctuations can be attributed to seasonal changes in nutrient availability, temperature and photoperiod, diatoms possess an intrinsic oscillation mechanism in their population due to their peculiar life cycle that interferes with external conditions. Thus, understanding the population dynamics of diatoms helps in understanding global carbon cycles.

In 1984, William M. Lewis of the University of Colorado described the unique life cycle of diatoms (Bacillariophyta) as "diatom sex clock".[6] Briefly, it comprises two alternating phases, a long mitotic size diminution phase and a short sexual size restoration phase. The uniqueness in size reduction and restoration is a consequence of the specific cell wall structure consisting of two biomineralized silica halves with different size (*epitheca* and *hypotheca*) that are assembled like a Petri dish. Upon cell division, each half becomes an *epitheca* of the next generation, in which a new *hypotheca* is synthesized. By this mechanism, the mean cell size of a population decreases from generation to generation, and the distribution of sizes becomes larger (MacDonald-Pfitzer rule).[7,8] Obviously, this process cannot proceed forever, so later generations undergo sexual reproduction and form haploid gametes which eventually fuse to diploid auxospores. Within these auxospores new large initial cells are produced, starting the cycle again. The variety of sexual mechanisms is large.[9,10] In some cases, auxosporulation can occur within one single cell (*uniparental*), whereas in other cases gametes from different cells have to recombine (*biparental*). Within these two main types, several variants are observed. In uniparental auxosporulation such as *automixis*, sexuality is reduced to some degree. Biparental (*allomictic*) auxosporulation can occur in *homothallic* species (gametes of both sexes are formed within a single clonal strain) or *heterothallic* species (strains of different mating types are required).[10] Von Stosch was able to show by experiments using artificial alteration of size that the threshold for sexual reproduction is determined by cell size rather than by age.[11,12] Therefore, a specific size range of cells that are capable of sexual reproduction can be assumed for each individual species. If the cell is larger than an upper sexual size threshold, auxosporulation is blocked.[13,10] In some cases, also a lower size limit for auxosporulation exist, the life cycle is then referred to as “closed”. In any case there is a minimum size until which the cells are viable.

Together with the maximum size of the initial cells, this defines the possible range for the cell size. It should be noted that while the size reduction-restitution mechanism is wide-spread and distinguishes diatoms from other taxa, exceptions are described showing no decrease in size during the vegetative phase or even vegetative enlargement in order to produce larger cells.[9,14] However, by the standard mechanism, as William Lewis pointed out, the diatom life cycle ("sex clock" or generation clock) defines its own rhythm independent from environmental constraints. Cell size reduction- restitution cycles that can last many years in natural environments, apparently support this hypothesis.[15]

There is a caveat, however, for taking the diatom sex clock simply as a periodic process, and that is caused by the broadening of the cell size distribution. If the size distribution broadens continuously and larger cells are maintained in the system, it is difficult to close the cycle and return to a previous state without any additional mechanisms that counteract this broadening. While this is certainly a challenge to the clock concept, field observations of diatom populations over many years confirm periodic fluctuations with the proposed periodicity of the life cycle.[15,16,17] Mathematical models may help in understanding the possible mechanisms that cause a deviation from the simple step-by-step size reduction-restitution scheme. Simulations have been made with a large set of parameters aimed at matching the experimental observations, notably in the work of Schwarz et al.,[18] D'Alelio et al.,[17] and Hense & Beckmann.[19] Schwarz et al.[18] fitted experimental data for *Pseudo-nitzschia delicatissima* with a continuous-time Markov chain model and investigated the stationary distribution without oscillations. D'Alelio[17] modelled the cell size dynamics of *Pseudo-nitzschia multistriata* over 11 years in an 8-parameter model with polynomial differential equations. The 14-parameter model of Hense and Beckmann[19] took the environment into account by modelling vertical migration in a water column. In their study, multimodal size distributions were attributed to intra- and interspecific competition as a way to overcome the broadening of the size distribution. With this contribution, we address this issue from a different perspective and ask under which circumstances real periodicity can be obtained in a discrete minimum model derived from the generation-resolved MacDonald-Pfitzer scheme and what are the obstacles and conditions for maintaining the clock over many periods.

2. Materials and Methods

We describe the state of a diatom population in the basic model (referred to as *basic linear model*) as a vector $\boldsymbol{x}$ of size n, in which each element represents the number of individuals of a distinct size

class per volume. The order of sizes is chosen such that higher indices characterize larger sizes and that we start with the index i=0 for the smallest size, leaving for the largest size (i.e. the initial cells) the index n-1. We adopt this enumeration convention starting with 0 (rather than 1) in order to be compatible with the programming language and algorithms used in the simulations.

Using different stages for a single species – a concept that we transfer here to the diatom life cycle – is known as the Leslie model[20] in biomathematical literature. Briefly, in the Leslie model a (female) animal population is divided into different age classes, typically 3, with separate transition rates to the next generation. Whereas the Leslie model and other models for population dynamics typically treat time as continuous variable, we account for the special proliferation mechanism with discrete size steps at discrete time points and model the system as a discrete dynamical system.[21] This means that we determine the population state at discrete points in time t, defining distinct generations in accordance with the MacDonald-Pfitzer rule. The transition from one generation to the next is thus expressed by a propagation matrix $\boldsymbol{P}$ applied to the current population state

$$\boldsymbol{x}_{t+1} = \boldsymbol{P}\,\boldsymbol{x}_t \quad . \tag{1}$$

The elements of this matrix are determined by the two states in the diatom life cycle. The vegetative phase is represented by the diagonal elements denoting daughters derived from the epitheca, and the upper side diagonal denoting daughters from the hypotheca. The probability of successful division and survival to the next generation is given as parameter p. In order to treat a possible bias between the two daughters in this probability, we multiply the diagonal elements by β. For size classes that are capable of auxosporulation, a different factor for remaining α is assigned. The sexual phase is represented by a parameter s, which defines the probability for the lower size classes to form auxospores and initial cells in the next step. With s in the lower left corner of the propagation matrix, the life cycle is closed. In order to be able to extract p from the propagation matrix and to simplify the resulting analytical expressions for general n, we write $s=\sigma^n p$ and conveniently use σ instead of s as parameter. For reference, all parameters are compiled in Table 1.

For simplicity and parameter reduction, we assume that only the smallest size class can undergo auxosporulation, thus contracting the corresponding size range lower than the upper threshold for auxosporulation to one single class. The propagation matrix of the basic linear model is thus given as

$$\boldsymbol{P}=\begin{pmatrix} \alpha p & p & 0 & \dots & 0 & 0 & 0 \\ 0 & \beta p & p & \dots & 0 & 0 & 0 \\ 0 & 0 & \beta p & \dots & 0 & 0 & 0 \\ \dots & \dots & \dots & \dots & \dots & \dots & \dots \\ 0 & 0 & 0 & \dots & \beta p & p & 0 \\ 0 & 0 & 0 & \dots & 0 & \beta p & p \\ s & 0 & 0 & \dots & 0 & 0 & \beta p \end{pmatrix} = p \begin{pmatrix} \alpha & 1 & 0 & \dots & 0 & 0 & 0 \\ 0 & \beta & 1 & \dots & 0 & 0 & 0 \\ 0 & 0 & \beta & \dots & 0 & 0 & 0 \\ \dots & \dots & \dots & \dots & \dots & \dots & \dots \\ 0 & 0 & 0 & \dots & \beta & 1 & 0 \\ 0 & 0 & 0 & \dots & 0 & \beta & 1 \\ \sigma^n & 0 & 0 & \dots & 0 & 0 & \beta \end{pmatrix} \quad (2)$$

Considering a whole size range and introducing an additional parameter as upper size threshold or even a distribution of initial sizes is possible and would give additional entries in the matrix. The corresponding expressions as shown in the Supplementary Information. We can safely ignore all classes smaller than a possible lower size threshold for auxosporulation, since they will not contribute further to the cycle and eventually die out.

In the basic linear model, the auxosporulation probability is proportional to the number of possible parent cells.

Table 1. Parameters used in the models

Parameter	Meaning	Model
n	number of size classes	all models
i	index for size class, $0 \le i < n$	all models
p	survival probability of theca	all models
s	probability of auxosporulation	all models
σ	$(s/p)^{1/n}$	all models
α	survival factor of smallest cell	all models
β	asymmetry factor between daughters	all models
t	generation as timescale	all models
γ	inverse carrying capacity	saturation models, ageing models
m	number of age classes	ageing models
j	index for age class, $0 \le j < m$	ageing models
z	period of a *zeitgeber* in generations	zeitgeber models

We note that a generation-resolved discrete matrix model without implementation of a sexual phase was used by Terzieva & Terziev,[22] whereas other previous models were based on differential equations, the one of Schwarz et al.[18] being also linear, others using polynomial or further nonlinear expressions.[17,19]

Four classes of variations of the basic linear model are considered:

First, possible delays of one generation caused by short resting phases in epitheca, hypotheca or auxospores are treated. They could be modelled with second order difference equations (delay difference equations[23]).

$$\boldsymbol{x_{t+1}=P_0 x_t+P_1 x_{t-1}} \tag{3}$$

but we rewrite this expression using a single matrix and state vectors of double size containing both $\boldsymbol{x_t}$ and $\boldsymbol{x_{t-1}}$ (see Supplementary Information 2). These variations are called *delay models.* In the *Müller delay model*, the smaller daughter is delayed by one generation, whereas in the *Laney delay model*, the larger daughter is delayed by one generation.

Second, a nonlinearity is introduced (*nonlinear models*). A biparental scheme for sexual reproduction was modelled by

$$x_{n-1,t+1}=\frac{s\,x_{0,t}^2}{(1+2\,s\,x_{0,t})} \quad (\textit{biparental nonlinear model}) \tag{4}$$

instead of

$$x_{n-1,t+1}=s\,x_{0,t} \tag{5}$$

as in the basic linear model.

In an independent nonlinear model, overpopulation was avoided by introducing a saturation limit for the population according to a Ricker function.[24] Extending the Ricker function to multiple size classes, p drops exponentially with the total number of cells according to

$$p=p_0\,e^{-\gamma\left(\sum_i x_i\right)_t} \quad (\textit{saturation nonlinear model}). \tag{6}$$

Saturation nonlinearity was also used in the following two classes of models.

Third, for simulating a finite life span (*ageing model*) we coded the age of the *epitheca* of a cell as an additional dimension of size m, representing m different age classes (index j with $0 \le j < m$). Hence, the state vector was replaced formally by a matrix of size $n \times m$, and the propagation matrix formally by a tensor of forth rank. In the analytical treatment (Supplementary Information 3), the state matrix was rewritten to a simple vector as in the case of the delay model, so that $\boldsymbol{P}$ could still be treated as a matrix. For the computational treatment, a fast algorithm was devised (Supplementary Information 5), taking advantage of the fact that only some elements differ from zero. The new population was then calculated as the sum of only two contributions: (a) cells from the epithecae, formed by shifting the previous population matrix *to the right* (increase of age by one), removing aged cells and correcting the remaining ones by the appropriate factors $\alpha\,p$ and $\beta\,p$; and (b) cells from the hypothecae, formed by shifting the previous population matrix *upwards*

(decrease in size). The matrix multiplication was therefore reduced to two “roll” commands. Additionally, new large cells from auxospores were considered. This computational trick had been applied in most simulations, also in implementations of the other models in which only the second roll was needed.

Forth, *p* or *s* are made variable in order to account for seasonal changes in growth and auxospore formation (*zeitgeber models*). A sinusoidal variation between a maximum and minimum value was assumed as basic mode. In the *p-zeitgeber model*, *p* is varied, whereas in the *s-zeitgeber model*, *σ* is varied.

For analysing all investigated cases, we used a combination of two methods, an analytical one and a computational one. Whenever possible, we performed a mathematical analysis in order to find the contributing eigenvalues and eigenvectors. If the eigenvalues λ_k and corresponding eigenvectors ξ_k of $\boldsymbol{P}$ are known, then for arbitrary initial conditions, the temporal evolution of the population after *t* generations can be predicted as a sum of distinct relaxation modes according to

$$\boldsymbol{x_t} = \boldsymbol{P^t}\,\boldsymbol{x_0} = \sum_k \lambda_k^t\, c_k\, \xi_k \quad . \tag{7}$$

Here, the coefficients c_i denote the decomposition of the initial vector $\boldsymbol{x_0}$ into contributing eigenvectors.

This analytical treatment is supplemented by computer simulations, especially in the cases where analytical expressions for the eigenvalues are not easily possible (saturation models, ageing model, zeitgeber models). Programs containing the different model variations were written in Python. Source codes are provided in Supplementary Information 5 and 7. In the computer simulations, we sampled as suitable measures for the population state at a certain point in time

the total number of cells $\quad N = \sum_{i=0}^{n-1} x_i \quad ,$ (8)

the number of formed auxospores $\quad A = s\,x_0 \quad ,$ (9)

the mean size (first moment of the distribution) $\quad M_1 = \frac{1}{N}\sum_i x_i\, i \quad ,$ (10)

and the variance $\quad V = M_2 - M_1^2$, derived from the second moment $\quad M_2 = \frac{1}{N}\sum_i x_i\, i^2 \quad .$ (11)

3. Results and discussion

Using different models, it is analysed under which assumptions oscillations of the population state are obtained, and whether these oscillations can be self-sustained or need external input. A sustained or driven oscillation with long periods would constitute a sex clock in the meaning attributed by Lewis to the diatom life cycle. We start with a linear model, then this model is extended systematically in order to demonstrate which changes have to be made in order to favour oscillatory behaviour. In contrast to multi-parameter models aimed at ecosystem simulations for matching field data,[17-19] the number of parameters is kept as small as possible to show the principle logic behind the mechanisms. The systematic approach of extracting analytical information from a linear model extended to delay and ageing processes, while being able to implement nonlinearities and *zeitgeber* by varying the parameters of the model computationally, is a unique feature that distinguishes our approach from previous reports.

3.1 Basic linear model

The basic linear model represents the original MacDonald-Pfitzer rule. With this model we can rigorously answer the question why the model needs a modification in order to explain sustained oscillations in the population distribution. The MacDonald-Pfitzer rule refers to distinct generations, thus the application of a discrete model with distinct time steps is well justified. We note that diatom cultures can even be synchronized (with the help of nutrient starvation or blue light[25]) which would allow an experimental verification of generation-resolved models. However, not enough data are available at the moment.

As explained in the Materials and Methods section, the population state consists of the number of cells for each size. In real species, up to 500 different sizes can be achieved with an average generation time of one week, resulting in life cycles of several years (Mann, 1988).[15] For understanding the generic behaviour of the model, the exact number of sizes is not important, though.

The main parameters used in the model are the vegetative proliferation probability p, the sexual proliferation probability s, an asymmetry factor between the daughter cells in the vegetative phase β, and a survival factor for the smallest cells α (see Table 1). In our basis model, all sizes that are capable of auxosporulation are contracted into this single size class. This approach seems to be a rough approximation, but we will show at the end of the section that the main conclusions also hold if we consider a distribution of sexual stages or initial cell sizes. By construction, the linear model

represents uniparental sexual schemes, but biparental schemes are covered as well in the limit of high cell density (see section 3.3).

The “ideal” case in which there are no losses of cells and doubling in the vegetative phase is characterized by the parameters $p = \beta = 1$, $\alpha = 0$ and $s = 1$. With one initial cell of largest size as the usual initial condition, the occupation numbers of the different size classes follow directly from Pascal's triangle (see Fig. 1a) with a total number of 2^t cells after t generations, up to the point where the smallest class is reached and new initial cells via auxosporulation are generated.

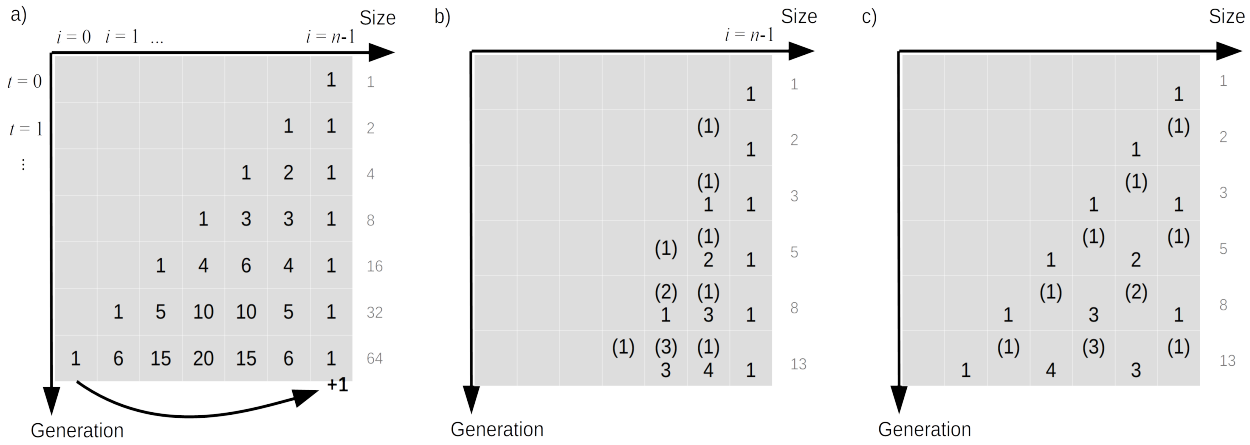

Figure 1. Three different models for the proliferation mechanism of diatoms a) simple binary fission (basic linear model) b) binary fission with a delay of one generation for the hypothecal daughter (Müller delay model). c) binary fission with a delay of one generation for the epithecal daughter (Laney delay model). Cells that cannot divide in the next generation are denoted with brackets. The total number of cells are counted in the columns on the right side (grey numbers).

The number of cells would be invariant if only half of the cells in the vegetative phase survived, i.e. $p = 0.5$, other parameters unchanged. For intermediate values of p, there is a value of s that on the long term balances the growth in the vegetative phase by loss in the sexual phase. In Fig. 2 a typical result is plotted for the linear model with parameters near to this steady state. It reflects the general behaviour obtained for this model: Oscillations in the output variables occur, but they decay and approach an equilibrium in the long term.

This behaviour can be attributed the continuous broadening of the size distribution which prevents a periodic transition of a narrow size peak through all size classes. In the physical language, such a transient wave without broadening would be described as a “soliton”.

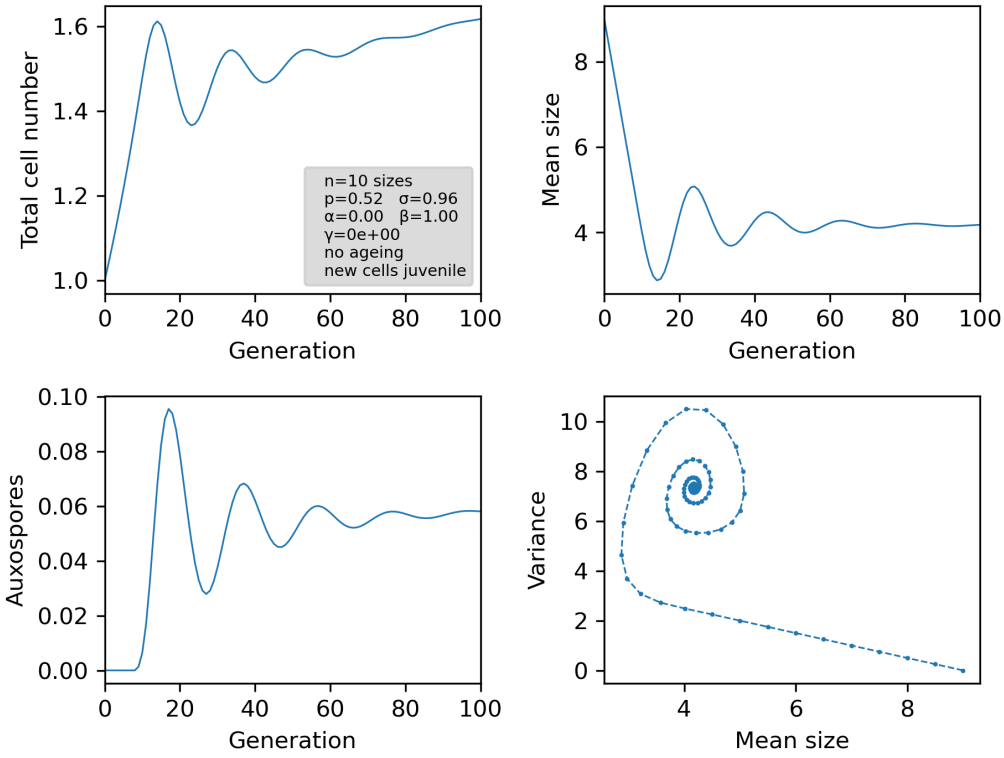

Figure 2. Results of the linear model with parameters near to a true steady state, characterized by a constant total cell number (per unit volume) as well as a constant population distribution.

Next, it is shown how the problem of the relaxation behaviour can be transformed into mathematical language. Doing this, we can prove rigorously that oscillations in the linear model will always decay regardless of the parameters, and which concepts for the mechanism will not be able to change this behaviour. The temporal evolution of the system is described by equation (5) and thus depends on the eigenvalues of the matrix **P**. The leading (dominant) eigenvalue λ_{max}, i.e. the one with largest absolute value, and its corresponding eigenvector will dominate the population in the long term, since contributions from all other eigenvalues are decaying faster (or not growing so fast). Oscillations in the population will be indicated by complex eigenvalues or negative real eigenvalues that indicate a cycle of two generations). Therefore, if the dominant eigenvalue *is not real positive*, we will find sustained oscillations. In all other cases intermediate oscillations will decay in the long term.

An answer whether sustained oscillations are possible or not can be given quite elegantly by the application of the Perron-Frobenius theorem.[26,27] It states that for non-negative irreducible matrices, the dominant eigenvector *is always* positive. Matrix **P** is non-negative because none of the matrix elements has a negative sign, and irreducible because it reflects a cyclic mapping of one row index

in the state vector to the next lower one and therefore exhibits a strong connectivity (for a mathematical proof see Supplementary Information 1). However, decaying oscillations exist and we can analyse the decay parameters represented by the non-leading eigenvalues.

For $\alpha=\beta$, the eigenvalues of $\boldsymbol{P}$ can be easily calculated for general dimension n (see Supplementary Information 1). They are evenly distributed in the complex plane on a circle around $p\,\beta$ with radius $r=p\,\sigma$. The dominant eigenvalue is located on the real axis. For odd n, this is the only real eigenvalue. For even n, there is a second one at $p(\beta-\sigma)$. It should be remarked that eigenvectors with negative eigenvalues may contribute but can never dominate, since for any non-negative initial vector a change of sign is prevented by the non-negative values in the matrix. An important case for the dominating eigenvalue is $\lambda_{max}=p(\beta+\sigma)=1$ that represents a stable population with zero growth. For each combination of β and σ there is exactly one corresponding value of p that leads to this condition. The number of cells is maintained with the eigenvalue of +1 and due to the symmetry, the eigenvector for this special case shows an equal distribution between all size classes. If $\sigma<1$, the dominant eigenvector represents an exponentially falling distribution from smallest to largest sizes, depending solely on σ irrespective of the value for β. The other eigenvalues with non-zero imaginary part describe oscillations. Since each trajectory starting from a certain initial state is a superposition of n possible relaxation modes, these oscillations are superposed to a decreasing, increasing or stable total population. Since the dominant eigenvector is always present in an initial vector with non-negative occupations, the contributions of these oscillations vanish in the long term.

The period T of the oscillations can be readily predicted. The eigenvalues have to applied T times to reach their original phase, so T is given by 360° divided by the angle of the eigenvalue to the real axis in the complex plane. Since the n eigenvalues are distributed evenly on a circle displaced from the origin by $p\,\beta$, this angle is smaller than $360°/n$. Thus, T is larger than n.

In the other limit for α, i.e. $\alpha = 0$, the situation is more complex and an analytical solution cannot be given easily. However, it is possible to find a relation between p, β and s such that a steady state with eigenvalue +1 results. For determining the generic case, we used the cofactor expansion method (see Supplementary Information 1) to obtain the determinant $|\boldsymbol{P}_n-\lambda\boldsymbol{I}|$ (I is the unity matrix). In short, the characteristic polynomial is given by

$$|\boldsymbol{P}_n-\lambda\boldsymbol{I}|=(p\alpha-\lambda)(p\beta-\lambda)^{n-1}-(-p\sigma)^n \quad . \tag{12}$$

Setting α to 0 and λ to +1, we can solve the roots for p for a given s, or calculate s for a given p via

$$s=\left(\frac{1-p\,\beta}{p}\right)^{n-1} \quad . \tag{13}$$

For a given *s*, the population-balancing value of *p* can be calculated analytically for *n*=2 and numerically for *n*>2. Valid solutions are real roots in the interval [0,1]. For *s*=0.5, *p* values depend on the dimension as follows: $p = 2\text{-}2\sqrt{2} \approx 0.586$ (*n*=3), 0.557 (*n*=4), 0.543 (*n*=5) 0.535 (*n*=6) ... With these specific relations between s and *p*, the number of cells as well as parameters of the distribution are time-invariant, thus we obtain a true equilibrium state.

The eigenvalues differ of course, but not too much from the eigenvalues in the case $\alpha=\beta$, with the same statements on periodicity. Indeed, the simulation in Fig. 2 reflects the deviation of the period from *n*.

The Perron-Frobenius theorem allows predictions for variations of the model in which other matrix elements are filled. For instance, we can consider a range of auxosporulating sizes below an upper size threshold or also a size distribution of initial cells depending on the parent cell size as observed by Davidovich.[28] The corresponding matrices still have only non-negative entries and retain their connectivity (see Supplementary information 1.3), so also in this case occurring oscillations will decay and are not self-sustained.

We can conclude that for a linear system oscillations occur but on the long term the trajectory spirals towards a stationary point, the population of which is represented by the dominant eigenvector. Therefore, the simple picture of the life cycle is not able to explain long-term oscillations in the population and size distribution.

3.2. Asymmetric delay

In this section we answer the question whether a delay in cell division between the daughter cells may cause sustained oscillations. Generally, delay processes are known to favour oscillatory behaviour in various contexts.[23,29] A delay for the smaller daughter by exactly one generation before the next cell division was suggested by O. Müller[30] in the early days of diatom research after careful studies on chain-forming *Melosira arenaria*. This asymmetry in time is not uncommon for single-celled organisms and is known for other species such as budding yeast[31] in which there is also a difference in size of the two mitotically separated cells. Interestingly, a delay of just the opposite sign was reported by Laney et al.[32] for the diatom *Ditylum brightwellii.* In this case the smaller daughter derived from the previous hypotheca is more likely to divide faster than the one from the

epitheca. These contradictory findings certainly express the need for more detailed experimental investigations and species-specific treatment. The variety of diatoms is so large that it is not known whether this asymmetry in timing between the two daughter cells holds for the majority of species or how this time delay can vary.

In both the Müller and Laney models with a delay of one generation, a Fibonacci series for the number of cells replaces the exponential growth. In Fig. 1b the principle is shown explicitly for the Müller model, in Fig. 1c for the Laney model. Without losses, the number of cells derived from one initial cell follows the series 1, 2, 3, 5, 8,... rather than 1, 2, 4, 8, 16 in the non-delayed scheme. Due to the delay the division scheme including closure by the sexual phase represents a second-order difference system, but it can be reduced to a first-order matrix equation as shown in Supplementary Information 2.

The resulting matrix for the Müller delay model is also non-negative and irreducible, thus the dominant eigenvalue is real positive and given for $\alpha=\beta$ by

$$\lambda_{\max}=\frac{\beta\, p}{2}\left(1+\sqrt{1+4\,\sigma/\beta}\right) \tag{14}$$

(see Supplementary Information 2).

That means that also with this division scheme the qualitative behaviour does not change, and no true oscillations can be expected. Indeed, simulations with this variant exhibit decaying oscillations similar to those in Fig. 2 (see Supplementary information 4). The timescale is larger, though, since the vegetative proliferation takes longer to cross all size classes (Fig. 1b). Again, an equilibrium population can be reached only with a special combination of the parameters, such that $\lambda_{max}=1$.

In the Laney delay model, the situation is somewhat different. Due to the transition into a resting phase and back, a short-term oscillation of 2 generations is induced (for even *n* this oscillation is sustained, see also Supplementary Information 4). In real cultures it would be difficult to observe such a behaviour, though, because even under high synchronization the delay would probably be subject to some distribution. Oscillations in the order of the life cycle decay as in the basic model, with the same timescale as can be deduced also from Fig. 1c. Sustained oscillations have not been found.

As a result from this section, we can conclude that a delay of one daughter cell with respect to further division changes the growth law of the population but does not stabilize oscillations in the life cycle.

3.3. Nonlinear processes

In this section we answer the question whether nonlinear processes can cause sustained oscillations. In modelling population dynamics, the assumption of limited resources that inhibit the growth of a population is a typical feature for underlying models. But also biparental schemes introduce a second-order nonlinearity by the required meeting probability of the two mating types. For the life cycle scheme of diatoms, we discuss biparental schemes first, and then nutrient saturation. Since linear eigenvalue analysis cannot be applied here, we performed computer simulations for the corresponding models, the *biparental nonlinear model* and the *saturation nonlinear model*.

Biparental reproduction should be modelled as second order kinetics similar to bimolecular chemical reactions, expressing the dependence on density of the mating strains as reported in literature.[33] We note, however, that there is a limit even in dense systems since the parent cells can only supply a limited number of gametes. Thus the number of auxospores cannot surpass the number of parent cells, so there will be a transition to first order with increasing cell number. Modelling a biparental scheme accordingly with the expression for the *biparental nonlinear model* (see Materials and Methods) results in a slight shift of the targeted equilibrium with time. Simulations showed decaying oscillations similar to the *basic linear model*, but no further stabilization of these oscillations. An illustrating example is given in Supplementary Information 4. The positive feedback that is introduced by the nonlinearity (more small cells produce more than proportionally auxospores) obviously is not able to counteract the size broadening mechanism. Sustained oscillations of the life cycle probably cannot be attributed to biparental nonlinearity. For the applicability of the models to different sexual reproduction schemes, however, we can conclude that the linear model is a good approximation also for biparental schemes.

Now, nutrient saturation is discussed. Limitation of nutrients (silica, nitrogen, iron, etc.) would reduce the growth of diatoms if the population is too large and therefore provide a kind of negative feedback. In selecting an appropriate nonlinear expression for saturation, measures have to be taken in a discrete model that the number of individuals will not fall below zero. Therefore, instead of assuming a logistic-type growth model,[34] which is the textbook model for discrete difference equations showing oscillations and chaos, we apply the nonlinear model of Ricker[35] and extend it here to our one-species-several-ages case. In the (one-dimensional) Ricker model, the proliferation rate drops exponentially down with the number of individuals as result of competition for nutrients, but can never become negative as in logistic growth. In our multidimensional model, we regard the

total number of cells as limiting factor for saturation, but note that in principle the total surface area or volume could also be considered. Written in terms of our matrix model, this means

$$\boldsymbol{x_{t+1}} = \boldsymbol{P}\,\boldsymbol{x_t}\, e^{-\gamma\left(\sum_i x_i\right)_t} \tag{15}$$

in which $\boldsymbol{P}$ is still the linear matrix (*saturation nonlinear model*). The sum in the exponent is over all elements of the population vector, i.e. counting the number of individuals.

In an alternate view on this model variation, we modify p into an effective p_{eff} depending on the total population

$$p_{eff} = p_0\, e^{-\gamma\left(\sum_i x_i\right)} \tag{16}$$

γ is the inverse of the number of cells K for which the proliferation rate drops to $1/e$ of the full rate, thus representing an inverse carrying capacity. If we compare this to the one-dimensional Ricker model written as

$$x_{t+1} = x_t\, e^r\, e^{-x/K} \tag{17}$$

with a critical value for the first bifurcation at r=2, it becomes clear that we can expect a similar bifurcation at a critical value of p, i.e. $p_{\text{crit}} = e^2/2 \approx 3.69$ (the factor 1/2 arises from the fact that one cell yields two cells in the next generation, thus $2p \equiv e^r$). Numerical simulations confirm this behaviour and show a decoupling of high-frequency oscillations due to nonlinearity from the cycle through the size classes. Figure 3 shows a representative simulation for $p = 4$. One can see on the one hand a persistent high-frequency oscillation in the total number of cells and on the other hand the damped oscillation of mean size and variance leading to a steady-state distribution. A stronger coupling of the nonlinear term to the dynamic size distribution can be achieved by defining the carrying capacity via the total cell surface or volume, but as respective simulations show, the general behaviour at the end of the simulation does not change. As long as there is an equilibrium distribution as attractor for the trajectory in the linear model, oscillating behaviour is controlled by the value of p, up to further bifurcations and eventually chaos. For the Ricker model, however, a p_{crit} of 3.69 for the onset of oscillations is too large to be reasonable, since in the biological model no cell can produce more than two daughter cells in the next generation (i.e. $p \leq 1$). It might be possible to redefine the time scale by assigning one discrete step to several generations at the cost of complicated proliferation schemes, but clearly the high frequency oscillations for large p values are not the oscillations we are looking for. It should be mentioned that we investigated several other

nonlinear models such as the three-parameter Hassell model,[36] and obtained similar results by detecting persistent oscillations only in the cell numbers, whereas oscillations in the size distribution still decay.

The effect of nonlinearity in providing an effective p to limit the total population can be seen best below the bifurcation onset. For instance, with n=5 (for better numerical accuracy), p=1, $\alpha=\beta=0.8$, $s=0.2$, $\gamma=10^{-3}$, an equilibrium population of 421.85 cells per volume was obtained, giving rise to $p_{\text{eff}}=0.656$ which perfectly fulfils the equilibrium condition

$$s_{\text{eff}}=\frac{s\,p_{\text{eff}}}{p}=\sigma^n\,p_{\text{eff}}=\frac{(1-p_{\text{eff}}\beta)^n}{p_{\text{eff}}^{n-1}} \tag{18}$$

expected for the linear system.

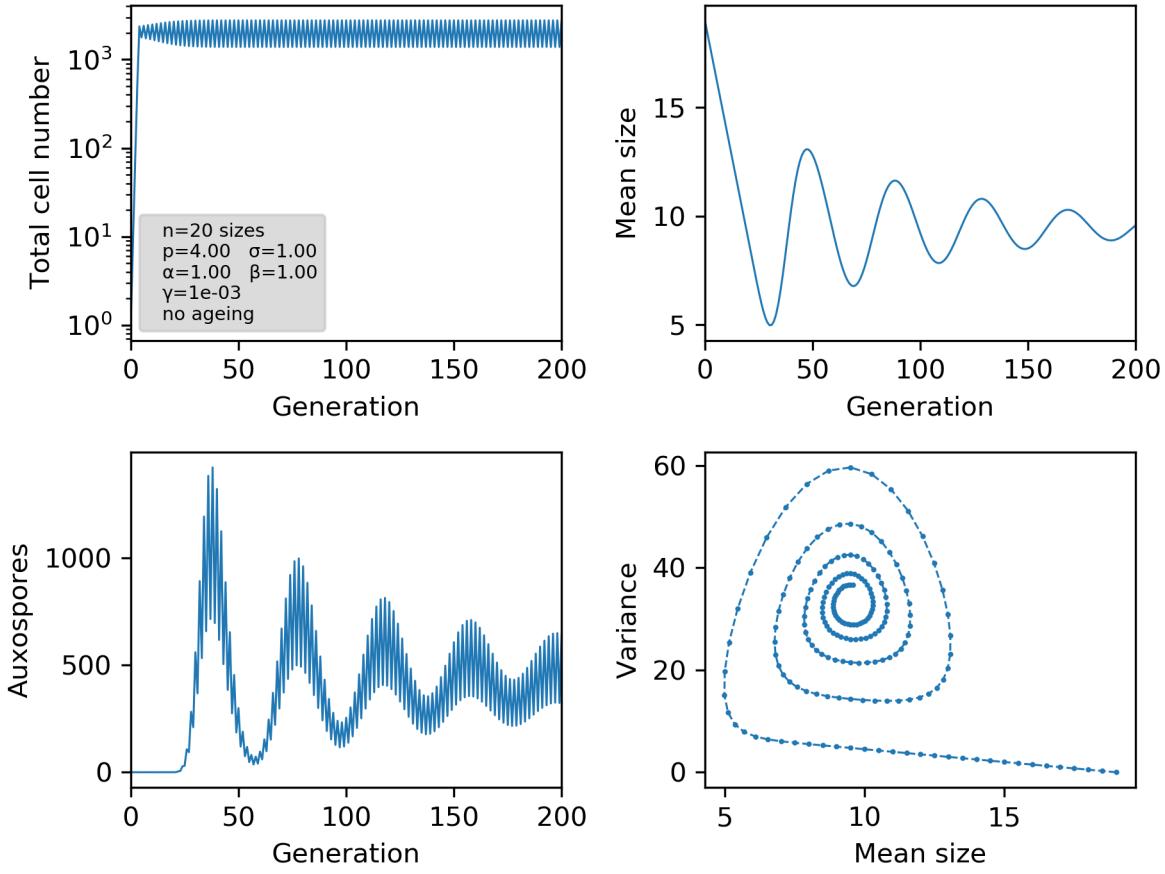

Figure 3. Results of a nonlinear Ricker model with a value for p exceeding the critical value for the first bifurcation. It can be seen that the high-frequency oscillation in the population (period 2) does not couple to the generation cycle (period around n).

As conclusion for the saturation nonlinearity, we can exclude this effect as cause for sustained oscillations with periods in the order of the number of generations. The simulations showed clearly

a decoupling of population control and size control. This did not change if we include the size in determining the saturation according to

$$p_{\text{eff}} = p\, e^{-\gamma\left(\sum_i x_i^2\right)} \quad \text{(total surface area)} \tag{19}$$

or

$$p_{\text{eff}} = p\, e^{-\gamma\left(\sum_i x_i^3\right)} \quad \text{(total cell volume volume)} \tag{20}$$

even if there is an explicit dependence on the size distribution.

3.4. Modelling with ageing

In this section we answer the question whether limited lifespans of individual thecae can cause sustained oscillations. The problem with all the models discussed up to this point is that a newly generated theca stays in the system and is not removed faster than thecae that are produced later. But in order to maintain a narrow distribution it is necessary that larger or older cells are removed. Thus a possible mechanism would be a limited lifespan of an epithecal half. Indeed there are some experimental reports addressing this issue, such as the one by D. Jewson for the centric diatom *Stephanodiscus neoastraea.* [37] Jewson deduced a lifespan of six to eight generations and extrapolated a similar value for *Aulacoseira subarctic*a.[38] Laney et al.[32] posed the hypothesis that by the bias to the smaller daughter cell damaged cell material can be divided asymmetrically, ensuring the quality of inherited material. The other, larger half will accumulate defects and eventually die earlier. This principle of genetic quality control by asymmetric cell divisions and implications for population development is found in several unicellular organism, for instance in *Escherichia coli* and in *Saccaromyces cerevisiae*, in which the asymmetry in cell division is much more pronounced.[31,39] For the latter it is known that one single mother cell can only produce 20-25 daughters by budding before dying which clearly defines a replicative lifespan. Budded daughters always start as juvenile cells independent of the age of the mother cell.[40]

Therefore we applied the *ageing model* in which the age of a cell is defined by the number of cell divisions its epitheca has already undergone. For sake of simplicity we define a fixed number of generations a theca may survive. Mathematically this means that the population is represented by an $n \times m$ matrix in which n (index i) denotes the number of size classes, and m (index j) defines the lifespan in generations. In order to keep the concept of a distinct lifespan meaningful, ageing for epithecae has to be more pronounced as for hypothecae. In our model, the smaller, “younger” cell

keeps its age, whereas the larger, “older” cell ages by one generation. When a cell reaches its lifespan after *m* generations, it is removed from the model.

We note that in the (biologically unrealistic) limiting case that only the hypothecal daughter survives in each cell division (lifespan = one generation), a perfect oscillation would be obtained. In this special case, the size for the single remaining cell would permute through all size classes until sexual reproduction would produce a single new initial cell.

Normally, we would assume that new initial cells are pristine, i.e. we set the age to zero. It is also instructive, however, to consider an alternative case in which new initial cells retain a memory of the age of their parent cells. Such a situation could hypothetically arise in the case of vegetative cell size enlargement in order to start the cycle again. Both possibilities are indicated in a small model system with *n*=4 and *m*=3 in Figure 4, indicating the very first generations.

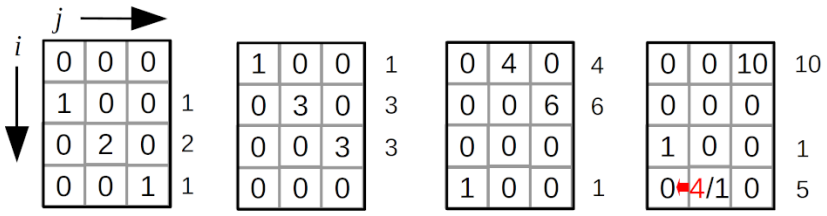

Figure 4. Age treatment of auxospores. *i* represents size class, *j* age. They retain their age or are set to pristine again (arrow). 4 sizes × 3 ages model, starting with 3rd generation. The narrowing distribution is indicated in the columns right to the matrices.

Pristine initial cells definitely consist the biologically more plausible case, so we confine our analytical treatment mainly to this case. We note, however, that in the case of an age memory upon re-entry of initial cells the conditions that mathematically prevent sustained oscillations are not fulfilled any more (Supplementary Information 3) and the process may become cyclic. Therefore, in the computer simulations both variations are treated for a comparison of these contrasting behaviour.

In order to analyse the results for arbitrary lifespans mathematically, we rewrote the state matrix as a vector of size *nm* and therefore the propagation as *nm* × *nm* matrix (see Materials and Methods section). Analytical treatment (Supplementary Information 3) lead to the following conclusions about the *nm* eigenvalues although an analytical expression for could not be given: First, 0 is a (*n*-1) (*m*-1) fold eigenvalue. Second, there is exactly one positive real eigenvalue. Again, for conservation of population number, this eigenvalue can be 1 for an exact combination of *p* (or p_{eff} in the case of

nonlinearity) and σ. Third, there are at most *m* negative real eigenvalues. That leaves a spectrum of minimum *nm*-(*n*-1)(*m*-1)-1-*m* = *n*-2 complex eigenvalues.

In order to see how they contribute to the time development of the population, simulations were performed. Respective results of a larger system are displayed in Figure 5 for the variant with age memory of initial cells and in Figure 6 for pristine initial cells. In all cases, a nonlinear Ricker term as explained above was implemented to keep an upper limit for the total number of cells.

If the auxospores retain their age, indeed sustained oscillations with a periodicity of the number of size classes are obtained (Fig. 5). This periodicity is induced by the circular character of the matrix and the constant removal of the generation formed *m* generations before. A closer look to the size distributions reveals that despite of stable oscillations a proper limit cycle in the sense of a cyclic propagation through a set of defined population states is not followed. Since the population distribution via Pascal's triangle is cut off after *m* values, the population becomes narrower from generation to generation. This can be seen in the variance plot of the simulations and in detail in the small model system of Fig. 4. The population becomes more and more dominated by the oldest size class. Thus, under the assumption of an "age memory" in the auxospore, an oscillation will not decay and is subject to self-narrowing of the distribution by the MacDonald-Pfitzer-process. At the moment, however, there is no hint that this assumption is justified in real diatom species.

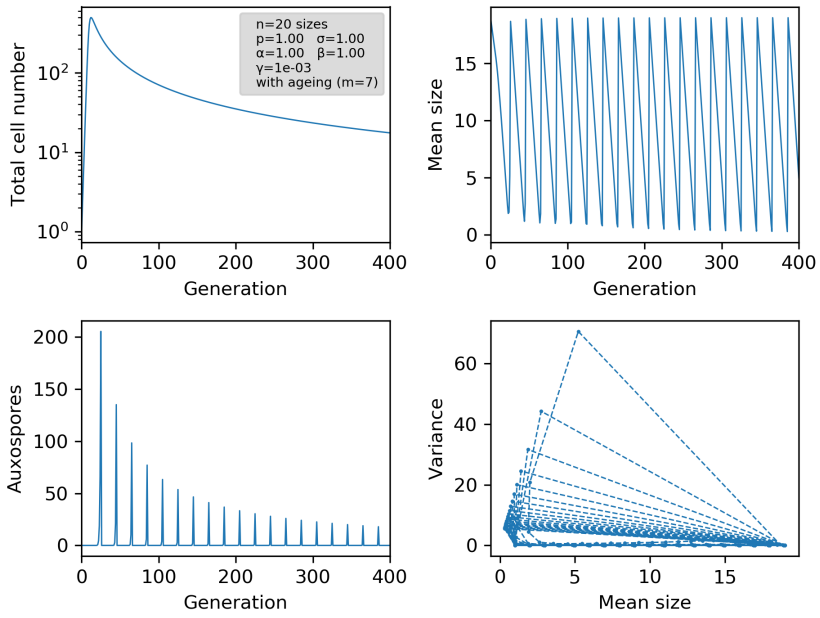

Figure 5. Results of a nonlinear ageing model in which auxospores carry a memory of the previous age.

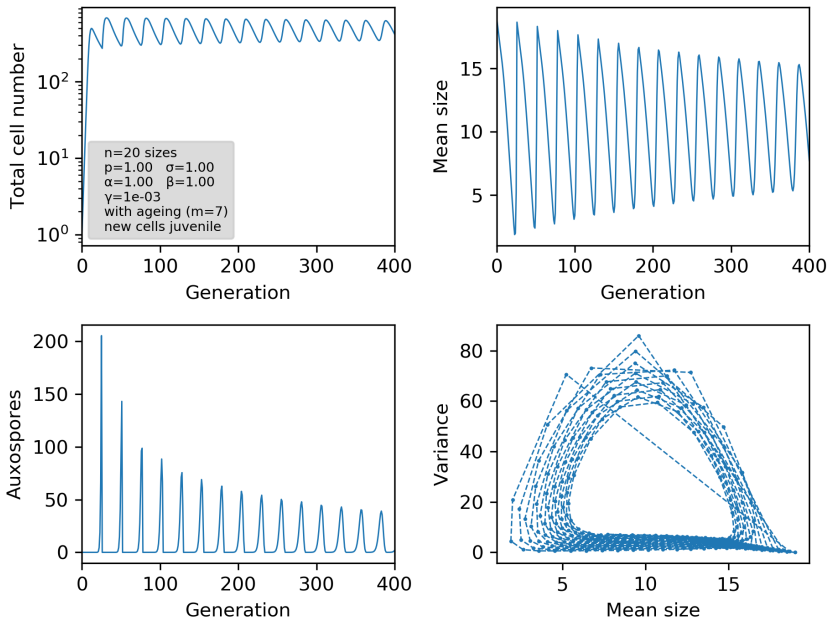

Figure 6. Results of a nonlinear ageing model in which auxospores are always pristine. In the lower right plot, the trajectory has to be read counterclockwise.

A different picture arises if new cells from auxospores are juvenile again. Here, the circular character of the propagation mechanism breaks down, and in each generation the re-entry of large, young cells is possible. This leads again to a smearing of the population distribution and results in a damped oscillation towards a steady state (Fig. 6). Due to the permanent reset of age, the distribution is smeared again, as indicated by the width of the auxospore peaks. An interesting feature arises also in the periodicity of the oscillations: now they deviate from the number of generations. Instead of the expected periodicity of 20 in Fig. 6, the periodicity in mean size, auxospore formation and variance is 26 generations for n=20 and m=7. This periodicity can be explained by considering the offspring of an auxospore until the next pristine auxospores is formed. The population moves diagonally through the $n \times m$ matrix, cells exceeding the right border being extinguished. After $n+m$-1 generations all cells derived from a single auxospore have disappeared, with the exception of the newly created auxospores (for details, see Supplementary Information 3). This $n+m$-1-periodicity has been confirmed in numerical simulations by computing the Fourier transform of the oscillations for various values of n and m. Only for a large m/n ratio, some small deviations are detected which we can attribute to a nonlinear distorsion and numerical uncertainties. A selection of simulated data are given in Table 2, the full dataset with various variations in the different model parameters are compiled in the Supplementary Information 6.

Table 2. Selection of simulation results under the assumption of a limited lifespan and juvenile initial cells. In all simulations $p = \alpha = \sigma = 1$, $\gamma = 0.001$. Given are the other parameters, average oscillation period in generations from Fourier transform, and fitting parameters for equilibrium distribution and relaxation of population maxima and minima as given in the text.

n	m	β	period	c_{max}	τ_{max}	c_{min}	τ_{min}	n_B	a	b
20	5	1	23.7	0.78	$1.3 \cdot 10^3$	0.96	$2.0 \cdot 10^3$	29.5	2.3	5.9
50	5	1	53.9	0.56	$19.0 \cdot 10^3$	0.98	$70.8 \cdot 10^3$	147.7	3.7	27.5
70	5	1	73.9	0.50	$47.4 \cdot 10^3$	0.98	$262.0 \cdot 10^3$	276.3	4.0	45.0
100	5	1	104.0	0.42	$111.2 \cdot 10^3$	0.97	$1049.6 \cdot 10^3$	531.0	4.3	71.6
140	5	1	144.0	0.36	$214.5 \cdot 10^3$	1.02	$3826.1 \cdot 10^3$	1342.6	4.7	157.5
50	2	1	51.0	0.72	$177.8 \cdot 10^3$	0.99	$330.6 \cdot 10^3$	133.3	1.7	8.8
50	4	1	52.9	0.56	$26.2 \cdot 10^3$	1.01	$102.4 \cdot 10^3$	150.1	3.1	22.9
50	8	1	56.8	0.65	$14.9 \cdot 10^3$	0.92	$32.8 \cdot 10^3$	127.3	5.3	32.1
50	12	1	60.6	0.80	$13.5 \cdot 10^3$	0.88	$16.9 \cdot 10^3$	100.5	6.6	27.3
50	20	1	68.2	1.04	$10.7 \cdot 10^3$	0.80	$6.7 \cdot 10^3$	68.7	6.4	13.0
50	5	1.9	54.0	0.45	$15.6 \cdot 10^3$	0.98	$125.8 \cdot 10^3$	244.3	4.2	65.8
50	5	1.4	53.9	0.50	$17.4 \cdot 10^3$	0.98	$96.1 \cdot 10^3$	192.4	4.0	44.2
50	5	0.8	53.9	0.60	$19.3 \cdot 10^3$	0.98	$57.5 \cdot 10^3$	124.4	3.4	19.6
50	5	0.5	53.8	0.71	$18.7 \cdot 10^3$	0.98	$36.3 \cdot 10^3$	89.1	2.8	9.2
50	5	0.2	53.5	1.01	$14.9 \cdot 10^3$	0.93	$13.4 \cdot 10^3$	58.8	1.5	2.2

In all simulations with pristine auxospores the oscillations decay towards an equilibrium state, but on a large timescale. Before discussing the interesting details of the long-term relaxation process, we will have a look on the equilibrium state, taken at the end of the simulations (after several million generations).

The presence of a defined equilibrium is ensured by the nonlinear Ricker term which controls the total population. From the structure of the $nm \times nm$ matrix that represents the linear operation on the population matrix, it can be shown that again only certain combinations of p – together with the nonlinear Ricker term as p_{eff} – and σ lead to an eigenvalue of 1, that means a stable population. The $n \times m$ matrix characterizing the population eigenstate expresses a distinct size and age distribution in each age class. Comparable with observables, however, are mainly the cumulated size distributions, summed over the age structure (Fig. 7). It turns out that the total distribution has a maximum at a specific size class. Age-resolved plots show that this distribution is dominated by the *oldest* cells. For younger cells, the distribution is shifted towards larger sizes, which may be counter-intuitive at first sight. However, considering the fact that older cells on average went through more size-reducing cell divisions, one can understand the reason behind this. In Fig. 4, where the size

distributions for different ages can be read as columns, the tendency can already be seen after a few generations.

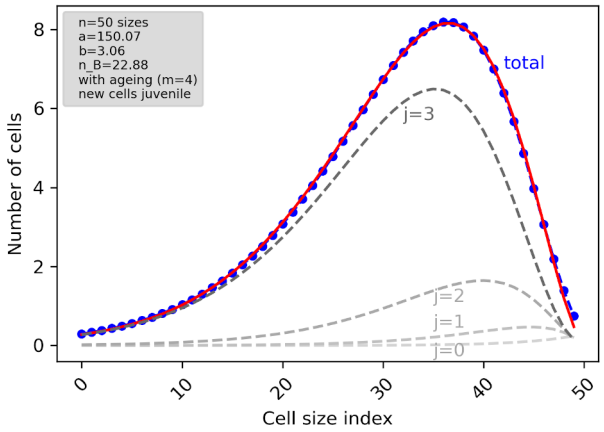

Figure 7. Equilibrium distribution after 5.3 mio. generations for distinct age classes and summed over all ages, with corresponding beta-binomial fitting functions. Simulation parameters are n = 50, m=4, p = α = β = σ = 1, γ = 0.001.

Fitting attempts with several distribution functions showed that it can be represented empirically by a beta-binomial distribution on an inverted size scale, i.e.

$$f(i)=\binom{n_B}{n-i}\frac{B(a+n-i,n_B+b-n+i)}{B(a,b)}(1-d)+d \qquad (21)$$

in which i is again the size index and $B(a,b)$ the beta distribution with shape parameters a and b. In probability distributions n_B would represent the upper limit, hence n, but here it can be regarded just as an additional fit parameter deviating from n and taking also non-natural values. d is an offset with renormalization and is negligible in most cases. The distribution function can thus only be taken as empirical function without some statistical foundation, but it describes the simulated data astonishingly well. Note that this equilibrium distribution differs substantially from the flat distribution function in the simple models. The fitted parameter data are included in Table 1. The maximum of the age-cumulated size distribution, calculated in percentage relative to the largest size, shifts towards larger cells for increasing n at constant m and towards smaller cells for increasing m at constant n. The width of the distribution, measured as full width at half maximum FWHM, decreases in both cases.

Now we consider the relaxation process from an initial condition towards this equilibrium. For this purpose we plotted the maxima as well as the minima of the total cell number in each oscillation vs. generation t. The decline does not follow a simple exponential law – which is understandable considering the nonlinear term and the existence of several complex eigenvalues – but can be

reasonably well described by a stretched exponential function, in mathematics also known as complementary cumulative Weibull function,

$$N = A_2 + (A_1 - A_2)\exp(-(t/\tau)^c) \tag{22}$$

in which A_2 denotes the equilibrium cell number, (A_1-A_2) the starting amplitude, τ the scale parameter and c the shape parameter. The scale parameter can be taken as measure of the mean decay time and is represented graphically as the inflection point when the generation is plotted on a logarithmic timescale (Fig. 8).

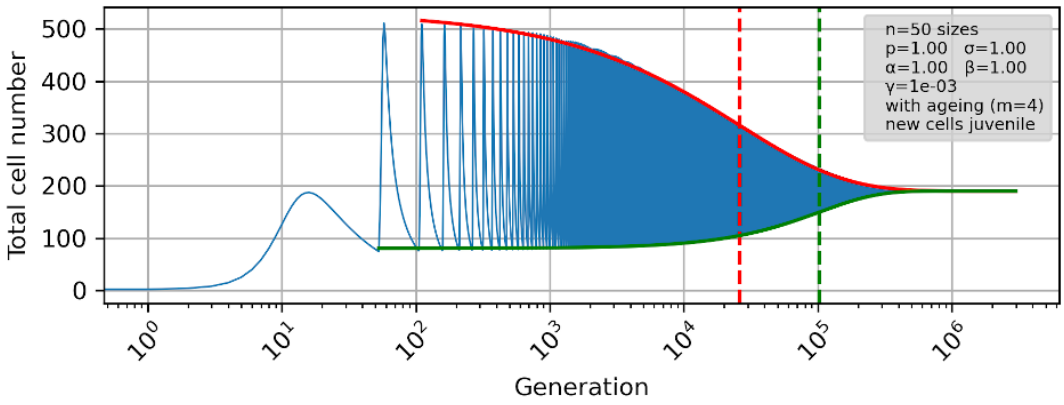

Figure 8. Relaxation of total cell number towards the equilibrium. Indicated are the enveloping stretched exponential fits for maxima and minima (thick solid lines) with the location of the inflection points (dashed lines). Note the logarithmic time scale. Simulation parameters are the same as in Fig. 7.

Fitted values describing the decline functions for various model parameters are also compiled in Table 1, with the full set in the electronic supplement. The following general trends can be extracted from the fits: For increasing number of size classes n, other parameters being constant, the equilibrium population decreases almost exponentially i.e. with positive curvature, the scale parameter τ increases with positive curvature. Interestingly, the shape parameter c decreases steadily for the maxima whereas it does not vary so much for the minima and passes through a transient maximum. For increasing lifespan m, other parameters being constant, the equilibrium population increases and the scale parameter decreases. The shape parameter increases for the maxima, but decreases for the minima. The higher the preference for younger daughter cells is, i.e. for decreasing values of β, the lower is the population and the scale parameter in the minima. The shape parameter for the decay of the maxima becomes higher. Interestingly, the scale parameter of the maxima and the shape parameter of the minima are maximized for certain values of β. Finally, a change in σ leads to modifications of the decay parameters for maxima and minima in opposite directions, respectively. In summary, the relaxation parameters have a complex dependence of the

model parameters, but long lasting relaxations (i.e. large scale parameters) are obtained for large n, small m, and high values of β.

Even if an equilibrium point exists, it may never be reached in a real diatom population in a reasonable amount of time. We note that the decay by persistent oscillations comprises many orders of magnitude, in the order of 10^4 to 10^5 generations in the maxima, and even more in the minima. This is much longer than any biological system can stay undisturbed by external influences, so for any practical reason the oscillation can be regarded as a persistent one. Any perturbation that changes the parameters for vegetative or sexual reproduction slightly would induce a new deflection from equilibrium and start the oscillation anew. Possible factors that may contribute in natural environments are light conditions, temperature, predator occurrence, and nutrient availability.

3.5. Periodic environmental influences

Fluctuating external factors can be of a periodic nature, typically following the seasons throughout a year. Photoperiod, temperature and nutrients change within a year and favour or disfavour the total growth of a diatom population. Sexual reproduction may only be limited to a few weeks in a year (Mann, 1988).[15] It can therefore be inferred that seasonal changes of environmental factors act as *zeitgeber* and are coupled to the inherent mechanism of the life cycle by varying the reproduction parameters. This can be expressed as non-autonomous system in which p or s is a periodic function of time. We investigate the influence of such an external *zeitgeber* on the oscillations of the previous model. As basic mode we assume a sinusoidal variation and note that other annual variations can be expressed as sum of the basic mode and its higher harmonics. Usually, a year is shorter than the complete life cycle and can be expressed by $z<n$ generations.

In Fig. 9a, the results of a computer simulation with the *p-zeitgeber model* is shown for a variation of p between the original value and 75% of that value in one year consisting of z=20 generations, with n=50 size classes. The oscillating behaviour seems complicated, especially in the seemingly random auxosporulation events, but Fourier analysis reveals the occurrence of the $n+m$-1 generation period of 54 generations (frequency 0.0185) as well as the seasonal period of 20 generations (frequency 0.05). Interestingly, besides the usual higher harmonics, new periodicities arise: the difference frequency at 0.0315 and the sum frequency at 0.0685 which can be attributed to nonlinear coupling of the two periodic processes since the Ricker term is still included. Like nonlinear saturation, the seasonal change of p couples only to the cell number, but not to the size distribution. If the simulation is performed further until 10^6 generations (Fig. 9b), oscillations in the total cell number remain, but have been decayed for the mean size, leading to an equilibrium size

distribution as in the other models. The only remaining Fourier components for the cell number are the 20 generation-period, now being dominant, and the 54 (n+m-1) generation-period.

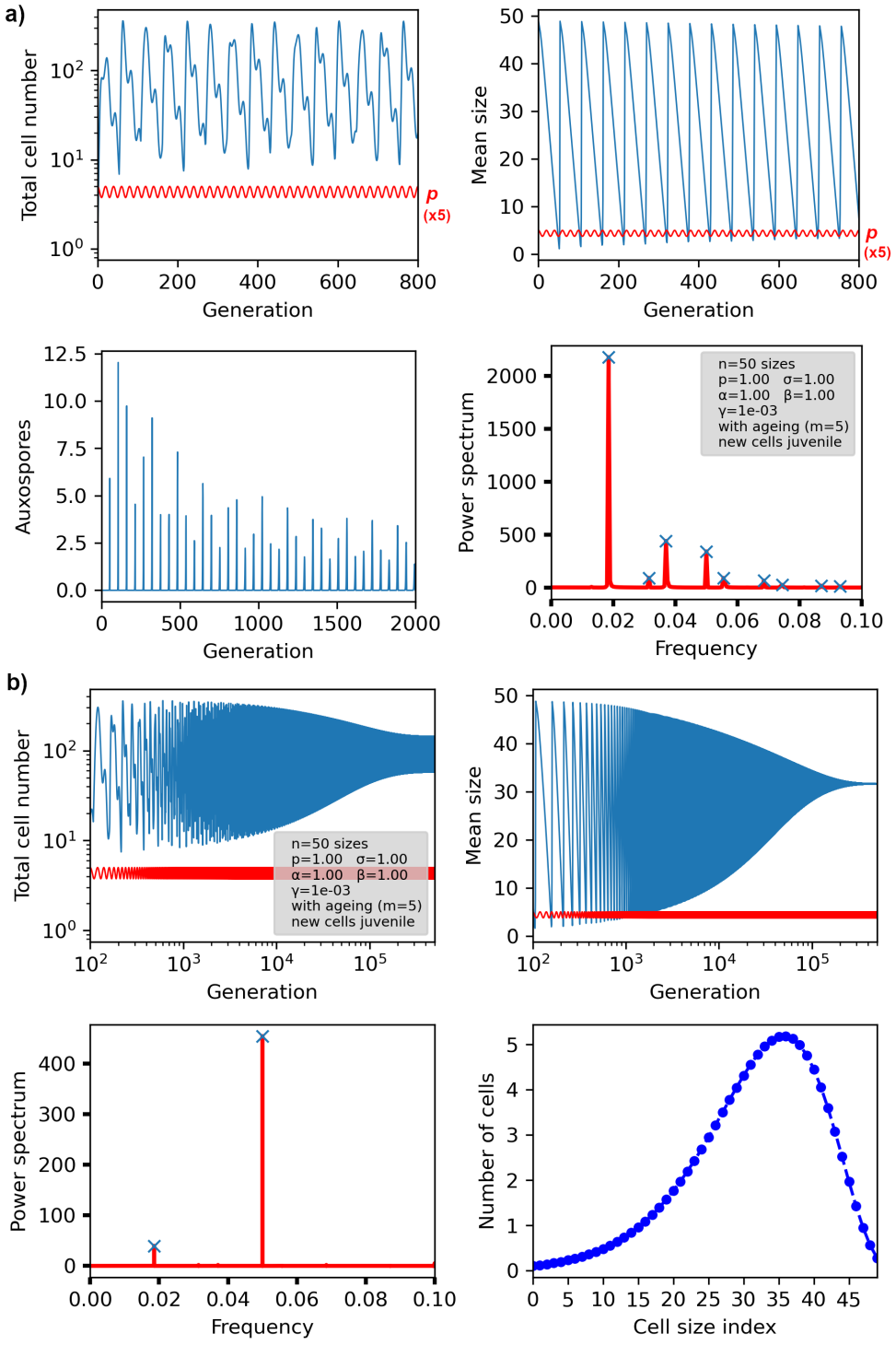

Figure 9. Simulation results for a system with sinusoidal variation of p down to 75% of its value, representing an annual *zeitgeber*. The nominal generation cycle (number of size classes) is n=50 generations, the *zeitgeber* cycle z=20 generations. (a) Behaviour at the beginning. Given is the total cell number, mean size, the auxospore number, and the

power spectrum of the total cell number. In both upper graphs, the sinusoidally varying value of *p* multiplied with a factor of 5 for better visibility is indicated as bottom line in red. (b) Long-term behaviour. Replacing auxospore number, the size distribution after 10^6 generations is displayed.

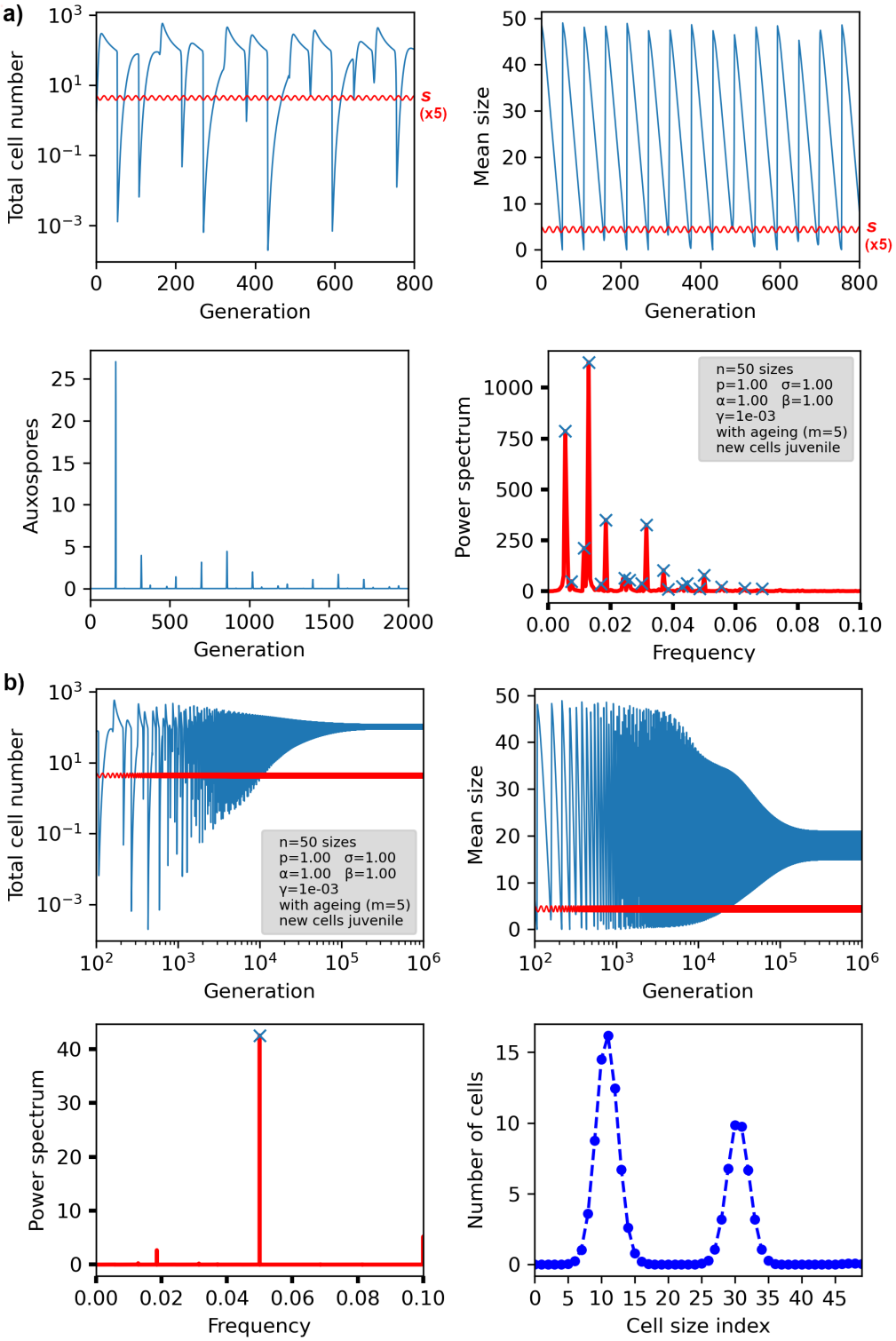

Figure 10. Simulation results for a system with sinusoidal variation of *s* down to 75% of its value. Graphs are displayed as in Fig. 9 at the beginning (a) and for 10^6 generations (b).

The situation is different if instead of *p*, *s* is varied since the variation concerns only the sexual part, i.e. the population of only the initial cells. In Fig. 10, the results are displayed for the same parameter set as in Fig. 9, but a variation of σ between the original value and 75% of that value (*s-zeitgeber model*). Since $s=p\sigma^n$, *s* drops down to virtually zero during the course of the year. Auxospore formation depends strongly on the phase relationship between total cell number and external signal, so there are some years in which there are almost no auxospores. The pattern in the frequency space at the beginning is much more complicated, with low frequency components indicating periodicities with long time scales, much longer than the generation period. After 10^6 generations, again the annual period dominates the population, but there is still an oscillaton in the meansize. The size distribution reveals the presence of a typical multimodal distribution (Fig. 10b, lower right), in which each peak can be attributed to a single year. These peaks traverse the size distribution, stabilizing the $n+m$-1 generation-period. Here, we can see clearly that a variation of *s* directly influences the cell size distribution and therefore keeps it oscillating, whereas a variation in *p* (Fig. 9) only influences the total cell number and therefore leads to the original equilibrium distribution. If there is no ageing, a multimodal distribution still exists, but is less narrow. The peak in the power spectrum for the $n+m$-1 vanishes which means that the *zeitgeber* signal defines the only remaining timescale (see Supplementary Information 4e).

We can state as result of this section that seasonally varying sexual reproduction behaviour may supply the necessary driving for keeping the generation clock running. Without ageing, however, the annual *zeitgeber* clock overwrites this clock completely and imprints its own rhythm.

4. Conclusion

Is the life cycle of diatoms a clock? If we mean limit cycles that consist of a series of defined population states that are adopted sequentially and return exactly back to previous states, then at the moment we would have to answer *no* with the present knowledge about the proliferation mechanism. The problem is the size distribution that needs some self-narrowing mechanism in order to compensate broadening exactly. If we assume finite lifetimes for a newly formed theca, then older, larger cells are removed effectively and counteract the broadening. With the additional assumption of age memory in auxospores, self-sustained rhythms with even further size narrowing can occur. But also without this somewhat arbitrary additional assumption, the oscillatory decay towards an equilibrium is significantly slowed down by the proposed finite lifetimes and takes place on a time scale of millions of generations, enough to keep the oscillations running by statistical fluctuations. If we define a biological clock in the common sense as “an inherent timing mechanism

in a living system that is inferred to exist in order to explain the timing or periodicity of various behaviours and physiological states and processes",[41] then the answer to our question is *yes*, but it resembles more a cuckoo clock that has to be wound up from time to time. This could happen by environmental fluctuations, ranging from singular environmental events bringing the size distribution again away from equilibrium up to the annual period of the sexual phase.

The results presented here may help in guiding experimental investigations of previously unknown or even contradictory data connecting cell cycle and life cycle. If for instance more data about the lifespan of a single theca and the asymmetry in timing between the daughters would be known, population dynamics of diatoms can be understood better. This may turn out useful – together with knowledge about nutrient supply currents – for modelling algal blooms and periodic events in the carbon cycle.

Author contributions

TF programmed the simulation code and wrote the major part of the manuscript. NK programmed the data analysis code and performed simulations. JZ performed literature research and checked available experimental data. RK introduced the concept of limited lifespan. WS performed matrix calculations and wrote the major part of the supplementary material.

Acknowledgments

The authors acknowledge fruitful discussions with the members of the Graduate School. We thank Aynura Mammadova for a preliminary treatment of the Ricker model.

Data Accessibility

All data including program code are given in the electronic supplementary material.

Funding Statement

This work was funded by the Graduate School on "Biological Clocks" P/979 and partially supported by the PhosMOrg consortium P/1052, both of the University of Kassel. The work of WS was supported by the bilateral project ANR-17-CE40-0036 and DFG-391322026 SYMBIONT.

References

1 Benoiston A-S, Ibarbalz FM, Bittner L, Guidi L, Jahn O, Dutkiewicz, Bowler C. 2017 The evolution of diatoms and their biogeochemical functions. *Phil. Trans. Roy. Soc. B: Biol. Sci.* **372**, 20160397 (doi: 10.1098/rstb.2016.0397)
2 Tréguer P, Bowler C, Moriceau B, Dutkiewicz S, Gehlen M, Aumont O, Bittner L, Dugdale R, Finkel Z, Iudicone D, Jahn O, Guidi L, Lasbleiz M, Leblanc K, Levy M, Pondaven P. Influence of diatom diversity on the ocean biological carbon pump. *Nature Geosci.* **11**, 27-37 (doi: 10.1038/s41561-017-0028x)
3 Nelson DM, Tréguer P, Brzezinski MA, Leynaert A, Quéguiner B. 1995 Production and dissolution of biogenic silica in the ocean: Revised global estimates, comparison with regional data and relationship to biogenic sedimentation. *Global Biogeochem. Cycles* **9**: 359-372
4 Smayda, TJ 1997 What is a bloom? A commentary. *Limnol. Oceanogr.* **42**, 1132-1136 (doi: 10.4319/lo.1997.42.5_part_2.1132)
5 Platt T, White GN, Thai L, Sathyendranath S, Roy S. 2009 The phenology of phytoplankton blooms: Ecosystem indicators from remote sensing. *Ecol. Model.* **220**, 3057-3069 (doi:10.1016/j.ecolmodel.2008.11.022)
6 Lewis WM. 1984 The diatom sex clock and its evolutionary significance. *Am. Nat.* **123**, 73-80
7 MacDonald JD. 1869 On the structure of the diatomaceous frustule, and its genetic cycle. *Annals and Magazine of Natural History* **3**, 1-8
8 Pfitzer E. 1869 Über Bau und Zellteilung der Diatomeen. *Botanische Zeitung* **27**, 774-776
9 Kaczmarska I, Pouličkova A, Sato S, Edlund M, Idei M, Watanabe T, Mann DG. 2013 Proposals for a terminology for diatom sexual reproduction, auxospores and resting stages. *Diatom research* **28**, 263-294
10 Chepurnov VA, Mann DG, Sabbe K, Vyverman W. 2004 Experimental studies on sexual reproduction in diatoms. *Int. Rev. Cytol.* **237**: 91-154
11 Von Stosch HA. 1965 Manipulierung der Zellgröße von Diatomeen im Experiment. *Phycologia* **5**, 21-44
12 Mann DG. 2011 Size and sex. In: Seckbach J, Kociolek JP (Eds.) Diatom World. Dordrecht: Springer, 145-166
13 Geitler L. 1935 Reproduction and life history in diatoms, *Bot. Rev.* **1**, 149-161
14 Gastineau R, Davidovich NA, Hallegraeff GM, Probert I, Mouget JL. 2014 Reproduction in Microalgae, in: Ramawat KG, Mérillon JM, Shivanna KR Reproductive Biology of Plants, Hoboken: CRC Press
15 Mann DG. 1988 Why didn't Lund see sex in Asterionella? A discussion of the diatom life cycle in nature. Algae and the aquatic environment. Biopress 384-412
16 Nipkow HF. 1927 Über das Verhalten der Skelette planktischer Kieselalgen im geschichteten Tiefenschlamm des Zürich- und Baldeggersees. Z. Hydrol. Hydrog. Hydrobiol. 4, 71-120
17 D'Alelio D, d'Alcalà MR, Dubroca L, Sarno D, Zingone A, Montresor M. 2010 A time for sex: A biennial life cycle in a marine planktonic diatom. *Limnol. Oceanogr.* **55**, 106-114
18 Schwarz R, Wolf M, Müller T. 2009 A probabilistic model of cell size reduction in Pseudo-nitzschia delicatissima (Bacillariophyta). *J. Theoret Biol.* **258**: 316-322
19 Hense I, Beckmann A. 2015 A theoretical investigation of the diatom cell-size reduction-restitution cycle. *Ecol. Model.* **317**, 66-82. (doi: 10.1016/j.ecolmodel.2015.09.003)
20 Leslie PH. 1945 On the use of matrices in certain population mathematics. *Biometrika* **33**, 183-212 (doi: 10.1093/biomet/33.3.183)
21 Sandefur JT. 1990 Discrete Dynamical Systems. Oxford, UK: Clarendon Press
22 Terzieva A, Terziev G. 2019 Model Diatom Population by Branching Stochastic Processes, *Appl. Comput. Mathem.* **8**, 3-8 (doi: 10.11648/j.acm.20190801.12)
23 Erneux T. 2009 Applied Delay Differential Equations. New York, US: Springer
24 Ricker WE. 1954 Stock and recruitment. J Fish. Res. Bd. Canada 11, 559-623
25 Huysman MJJ, Vyverman W, De Veylder L. 2014 Molecular regulation of the diatom cell cycle. *J. Exp. Bot.* **65**:2573-2584
26 Perron O. 1907 Zur Theorie der Matrizen. *Math. Ann.* **64**, 248-263
27 Frobenius G 1912 Über Matrizen aus nicht-negativen Elementen. *Sitzungsber. Kgl. Preuss. Akad. Wiss.* **1912**: 456-477
28 Davidovich NA. 1994 Factors controlling the size of initial cells in diatoms. *Russ. J. Plant Physiol.* **41**, 220-224
29 Novák B, Tyson JJ. 2008 Design principles of biochemical oscillators, *Nat. Rev. Mol. Cell. Biol.* **9**, 981-991 (doi: 10.1038/nrm2530)
30 Müller O. 1883 Das Gesetz der Zellteilungsfolge von *Melosira (Orthosira) arenaria* Moore. *Ber. Deut. Bot. Ges.* **1**, 35-44
31 Hartwell LH, Unger MW. 1977 Unequal division in Saccharomyces cerevisiae and its implications for the control of cell division, J. Cell Biol. 75, 422-435
32 Laney SR, Olson RJ, Sosik HM. 2012 Diatoms favor their younger daughters. *Limnol. Oceanogr.* **57**, 1572-1578
33 Scalco E, Stec K, Iudicone D, Ferrante MI, Montresor M. 2014 The dynamics of sexual phase in the marine diatom *Pseudo-nitzschia multistriata* (*Bacillariophyceae*), *J. Phycol.* **50**, 817-828
34 May R. 1976 Simple mathematical models with very complicated dynamics. *Nature* **261**, 459-467

References

35 Ricker WE. 1954 Stock and recruitment. J Fish. Res. Bd. Canada 11, 559-623
36 Geritz SAH, Kisdi É. 2004 On the mechanistic underpinning of discrete-time population models with complex dynamics, *J. Theor. Biol*. **228**, 261-269
37 Jewson DH. 1992 Life cycle of a Stephanodiscus sp. (Bacillariophyta). *J. Phycol*. **28**:856-866
38 Jewson DH. 1992 Size reduction, reproductive strategy and the life cycle of a centric diatom. *Phil. Trans. R. Soc. Lond*. B **336**, 191-213
39 Porro D, Cai M, Vanoni M, Alberghina L, Hatzis C. 2009 Analysis and Modeling of Growing Budding Yeast Populations at the Single Cell Level. *Cytometry* **75A**, 114-120
40 Steinkraus KA, Kaeberlein M, Kennedy BK. 2008 Replicative aging in yeast: the means to the end. *Rev. Cell. Dev. Biol*. **24**:29-54
41 Merriam-Webster.com Dictionary “Biological clock”, https://www.merriam-webster.com/dictionary/biological%20clock, Merriam Webster. Accessed 30 Oct. 2020

Supplementary Information

1 Basic Linear Model

We consider the propagation matrix P_n of our basic linear model without delay or internal structure and obtain for $s = \sigma^n p$ the $(n \times n)$-matrix

$$P_n = p \begin{pmatrix} \alpha & 1 & & & \\ & \beta & 1 & & \\ & & \ddots & \ddots & \\ & & & \beta & 1 \\ \sigma^n & & & & \beta \end{pmatrix} . \tag{1}$$

Recall that all three parameters β, p and σ take their values in the real interval $[0, 1]$ and we have $0 \leq \alpha \leq \beta$. We assume in the sequel that β, p and σ are different from 0, as this is the biologically most interesting case.

The matrix P_n is obviously (elementwise) nonnegative. We associate with it a directed graph G_n with vertices $1, \ldots, n$ and an edge from vertex i to j, whenever the entry of P_n at position ij is positive. Thus the graph G_n is of the following form:

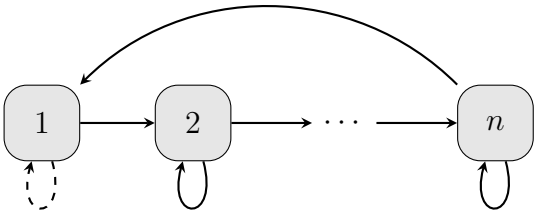

As one can see, G_n contains one loop of length n going through all vertices. This implies that G_n is a strongly connected graph where one can reach from any vertex any other vertex. By a well-known theorem,[1] this implies that P_n is an irreducible matrix. In addition, G_n contains loops of length 1 connecting the vertices $2, \ldots, n$ with themselves (for $\alpha \neq 0$ such a loop also exists for the vertex 1). The period of the matrix P_n is defined as the greatest common

[1] For a general survey of the theory of nonnegative matrices see Berman A., Plemmons R.J. 1994 Nonnegative Matrices in the Mathematical Sciences, SIAM, Philadelphia.

divisor of the lengths of the loops in G_n and hence we are dealing with an aperiodic matrix.

We can now apply the Perron-Frobenius theorem.[2] It asserts for a non-negative irreducible aperiodic matrix like P_n the following properties. Let $r > 0$ be the maximal modulus of an eigenvalue of P_n. Then r itself is a simple eigenvalue and it is the dominant eigenvalue, as the moduli of all other eigenvalues are less than r. Furthermore, there exists an eigenvector v to this eigenvalue r for which all entries are positive. If we assume that v is normalised such that the sum of all its entries is 1, then it describes the asymptotic behaviour of our discrete dynamical system $x_t = P_n^t x_0$ for almost all initial values: if x_0 is not an eigenvector, then we find for $t \to \infty$ that $x_t/\|x_t\| \to v$ where $\|x_t\|$ denotes the sum of the absolute values of the entries of the vector x_t.

1.1 Stationary state in the general case

The eigenvalues of the matrix P_n are the zeros of its characteristic polynomial $\chi_n(\lambda) = \det(P_n - \lambda I_n)$ where I_n denotes the $n \times n$ unit matrix. In our case, the determinant can be easily computed by expanding along the first column which has only two non-zero entries:

$$\begin{aligned}\chi_n(\lambda) = (p\alpha - \lambda) &\begin{vmatrix} p\beta-\lambda & p & & & 0 \\ & \ddots & \ddots & & \\ & & & p\beta-\lambda & p \\ 0 & & & & p\beta-\lambda \end{vmatrix} \\ &+ (-1)^{n-1} p\sigma^n \begin{vmatrix} p & & & & 0 \\ p\beta-\lambda & p & & & \\ & \ddots & \ddots & & \\ 0 & & & p\beta-\lambda & p \end{vmatrix} \qquad (2) \\ &= (p\alpha-\lambda)(p\beta-\lambda)^{n-1} - (-p\sigma)^n \,.\end{aligned}$$

From the above expression for the characteristic polynomial, it follows

[2] Perron O. 1907 Zur Theorie der Matrizen. Math. Ann. 64(2): 248–263. Frobenius G. 1912 Über Matrizen aus nicht negativen Elementen. Sitzungsber. Kgl. Preuss. Akad. Wiss. 1912: 456–477.

immediately that 1 is an eigenvalue, if and only if

$$s = \sigma p^n = (1 - p\alpha) \left(\frac{1 - p\beta}{p} \right)^{n-1} . \tag{3}$$

Thus for each choice of α, β and p there exists exactly one value for s leading to a stationary point.

1.2 Eigenvalues in the special case $\alpha = \beta$

If we denote as usual by $\zeta_k^{(n)} = e^{2\pi ki/n}$ for $0 \leq k \leq n-1$ the nth roots of unity, i. e. the n distinct complex solutions of $x^n = 1$, then it is easy to see that in this special case χ_n has n distinct zeros given by

$$\lambda_k = p(\beta + \zeta_k^{(n)} \sigma) \qquad 0 \leq k \leq n-1 . \tag{4}$$

The eigenvalues of the propagation matrix P_n are given by $\lambda_k = p\mu_k$. Thus in the complex plane, the eigenvalues of P_n lie uniformly on a circle with center $p\beta$ and radius $p\sigma$. If n is odd, then only the eigenvalue $\lambda_0 = p(\beta + \sigma)$ is real. For even n, also the eigenvalue $\lambda_{n/2} = p(\beta - \sigma)$ is real.

Oscillatory modes with a constant amplitude occur in a linear discrete dynamical system only, if the propagation matrix possesses at least one eigenvalue with absolute value 1. For our system, we find $|\lambda_k| = 1$, if

$$\beta^2 + \sigma^2 + 2\beta\sigma \cos(2\pi k/n) = 1/p^2 . \tag{5}$$

This condition can only be satisfied, if $\beta + \sigma \geq 1/p$. In the special case $\beta + \sigma = 1/p$, we must have $k = 0$ and we then find $\lambda_0 = 1$ corresponding to a stationary point. Writing $\phi = 2\pi k/n$ and considering (5) as an equation for σ, we find that for given $\beta \leq 1$ and ϕ this equation has a unique positive root, namely

$$\sigma = -\beta \cos\phi + \frac{1}{p} \sqrt{1 - p^2\beta^2 \sin^2\phi} \tag{6}$$

taking its values between 0 and 2. The real part of the corresponding eigenvalue is then given by

$$\mathrm{Re}(\lambda_k) = p(\beta + \sigma \cos\phi) . \tag{7}$$

Since for $k > 0$ the eigenvalue λ_k is not of maximal absolute value and thus not dominant, the corresponding oscillatory mode can be observed only for

carefully prepared initial values and thus is irrelevant as a model for nature. We may therefore conclude that our basic model does not support stable oscillations. Any oscillatory mode will either decay or grow exponentially.

A positive eigenvector for the dominant eigenvalue $\lambda_0 = p(\beta + \sigma)$ can be easily determined and is given by the vector

$$v = \begin{pmatrix} 1 \\ \sigma \\ \vdots \\ \sigma^{n-1} \end{pmatrix} \qquad \text{with norm} \qquad \|v\| = \frac{1-\sigma^n}{1-\sigma} \; . \tag{8}$$

Thus for almost all initial conditions the asymptotic distribution of the population over the different sizes is exclusively determined by the value of $\sigma = \sqrt[n]{s/p}$ and thus is in particular independent of β.

1.3 Linear Models with a Size Range for Auxosporulation

In the model considered in the previous section, all cells below a certain size threshold have been put into one size class, the only class where auxosporulation occurs. In this brief section, we comment on what happens, if we drop this simplifying assumption. There are (at least) two natural possibilities to implement a size range for auxosporulation. In the first one, cells generated by auxospores have always the maximum size. Abbreviating $\bar{\sigma} = 1 - \sigma^n$, we obtain then as propagation matrix instead of P_n the following matrix:

$$P'_n = p \begin{pmatrix} \alpha & \bar{\sigma} & & & & & & & \\ & \beta\bar{\sigma} & \bar{\sigma} & & & & & & \\ & & \ddots & \ddots & & & & & \\ & & & \beta\bar{\sigma} & \bar{\sigma} & & & & \\ & & & & \beta\bar{\sigma} & 1 & & & \\ & & & & & \beta & \ddots & & \\ & & & & & & \ddots & \ddots & \\ & & & & & & & \beta & 1 \\ \sigma^n & \dots & \dots & \dots & \sigma^n & 0 & \dots & 0 & \beta \end{pmatrix} .$$

If the k smallest size classes are able to form auxospores, then we have in the bottom row k times an entry σ^n. We omit a plot of the directed graph G'_n

associated to P'_n, as compared to the graph G_n only some additional edges appear. We have seen in the last section that G_n is strongly connected and hence the same is true for G'_n. It is also easy to see that the matrix P'_n is still aperiodic. Hence we can again apply the Perron-Frobenius theorem.

The second possibility is that the size of the cells generated by auxospores depends on the size of the parent cell. Now we obtain as propagation matrix

$$P''_n = p \begin{pmatrix} \alpha & \bar{\sigma} & & & & & & & \\ 0 & \beta\bar{\sigma} & \bar{\sigma} & & & & & & \\ \vdots & & \ddots & \ddots & & & & & \\ 0 & & & \beta\bar{\sigma} & \bar{\sigma} & & & & \\ \sigma^n & & & & \beta\bar{\sigma} & 1 & & & \\ & \ddots & & & & \beta & \ddots & & \\ & & \ddots & & & & \ddots & \ddots & \\ & & & \ddots & & & & \beta & 1 \\ & & & & \sigma^n & 0 & \dots & 0 & \beta \end{pmatrix} .$$

If we assume that $2k \leq n+1$, then the directed graph G''_n associated with P''_n possesses the following form:

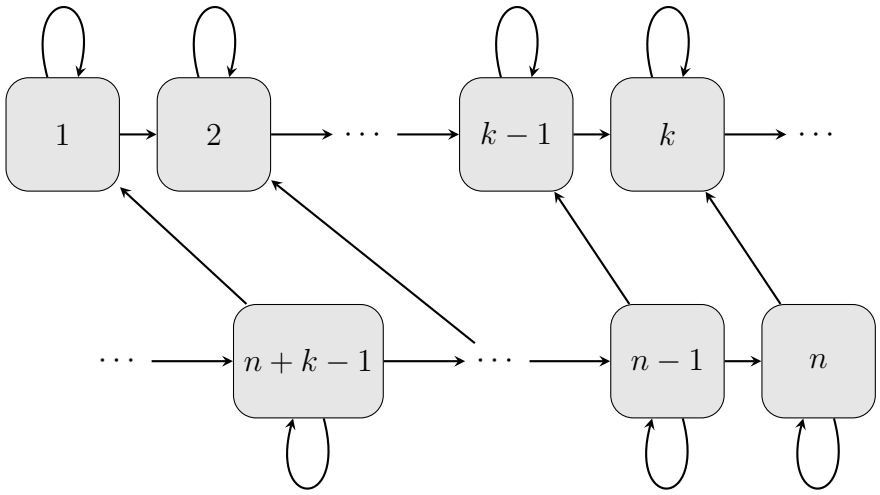

There exists a path visiting all nodes, namely

$$1 \to 2 \to \cdots \to n \to k \to k+1 \to \cdots \to n-k+1 \to 1 .$$

Hence the matrix P_n'' is irreducible. Because of the loops of length 1, it is also trivially aperiodic and we can again apply the Perron-Frobenius theorem.

If $2k > n+1$, one obtains exactly the same results, only the path visiting all nodes is slightly different. Once one has reached the vertex n, one must follow as many "backwards" arrows as neccessary to reach a vertex with an index less or equal $n-k+1$. From there, one walks "forward" to $n-k+1$ and then one can return to 1.

2 Linear Models with Delay

2.1 The Müller Model

We perform now a similar analysis for the delay model in the case where the smaller daughter needs one generation until it can reproduce, i. e. the model proposed by Müller. In this case, the linear model is a second-order difference system

$$x(t+1) = pA_0x(t) + \beta p^2 A_1 x(t-1) \tag{9}$$

where the coefficient matrices are given by

$$A_0 = \beta I_n\,, \qquad A_1 = \begin{pmatrix} 0 & 1 & & \\ & \ddots & \ddots & \\ & & 0 & 1 \\ \sigma^n & & & 0 \end{pmatrix} \tag{10}$$

where I_n is again the $n \times n$ identity matrix. We transform this system into a first-order one with twice the dimension by rewriting it in the form

$$\begin{pmatrix} x(t+1) \\ x(t) \end{pmatrix} = \begin{pmatrix} \beta p I_n & \beta p^2 A_1 \\ I_n & 0 \end{pmatrix} \begin{pmatrix} x(t) \\ x(t-1) \end{pmatrix} = P_{2n} \begin{pmatrix} x(t) \\ x(t-1) \end{pmatrix}\,. \tag{11}$$

Again the first task consists of determining the eigenvalues of the $2n \times 2n$ propagation matrix P_{2n}. For this, we use the following trick exploiting the block structure of P_{2n}. Assuming that A, B, C, D are square matrices of suitable, not necessarily equal sizes with A invertible and denoting generically by I identity matrices of the right size, the simple identity

$$\begin{pmatrix} A & B \\ C & D \end{pmatrix} \begin{pmatrix} I & -A^{-1}B \\ 0 & I \end{pmatrix} = \begin{pmatrix} A & 0 \\ C & D - CA^{-1}B \end{pmatrix}$$

implies that

$$\det\begin{pmatrix} A & B \\ C & D \end{pmatrix} = \det(A)\det\left(D - CA^{-1}B\right). \tag{12}$$

Hence, we can reduce the computation of the block determinant to computing two smaller determinants.

For determining the eigenvalues of the propagation matrix P_{2n}, we must compute $\det(P_{2n} - \lambda I_{2n})$ and therefore choose $A = pA_0 - \lambda I_n = (p\beta - \lambda)I_n$ (which is invertible over the field $\mathbb{R}(\lambda)$ of rational functions in λ), $B = \beta p^2 A_1$, $C = I_n$ and $D = -\lambda I_n$. Since A is a diagonal matrix, it is trivial to determine its inverse, $A^{-1} = (p\beta - \lambda)^{-1} I_n$, and its determinant is given by $\det(A) = (p\beta - \lambda)^n$. The second determinant in (12) takes the form

$$\det\left(D - CA^{-1}B\right) = (-1)^n \begin{vmatrix} \lambda & \frac{\beta p^2}{p\beta-\lambda} & & \\ & \lambda & \ddots & \\ & & \ddots & \frac{\beta p^2}{p\beta-\lambda} \\ \frac{\beta p^2 \sigma^n}{p\beta-\lambda} & & & \lambda \end{vmatrix}.$$

It can be easily computed by expanding along the first column and we obtain

$$\det\left(D - CA^{-1}B\right) = (-1)^n \left(\lambda^n - (-1)^n \left(\frac{\beta p^2 \sigma}{p\beta - \lambda}\right)^n\right).$$

Putting everything together, the characteristic polynomial of the propagation matrix P_{2n} can be written as

$$\chi_{2n}(\lambda) = \lambda^n (\lambda - p\beta)^n - \beta^n p^{2n} \sigma^n .$$

Hence we can express the eigenvalues of P_{2n} as n pairs of the form

$$\lambda_{k,\pm} = \frac{p}{2}\left(\beta \pm \sqrt{\beta^2 + 4\zeta_k^{(n)} \beta\sigma}\right)$$

where again $\zeta_k^{(n)}$ denotes for $1 \le k \le n$ the n different nth roots of unity. The dominant eigenvalue is $\lambda_{0,+} = \beta p(1 + \sqrt{1 + 4\sigma/\beta})/2$. The eigenvalue $\lambda_{0,-}$ is also real and if n is even, then the eigenvalues $\lambda_{n/2,\pm}$ are real, too. All other eigenvalues are complex.

Again the propagation matrix P_{2n} is nonnegative, irreducible and aperiodic. The associated direct graph G_{2n} has the following form:

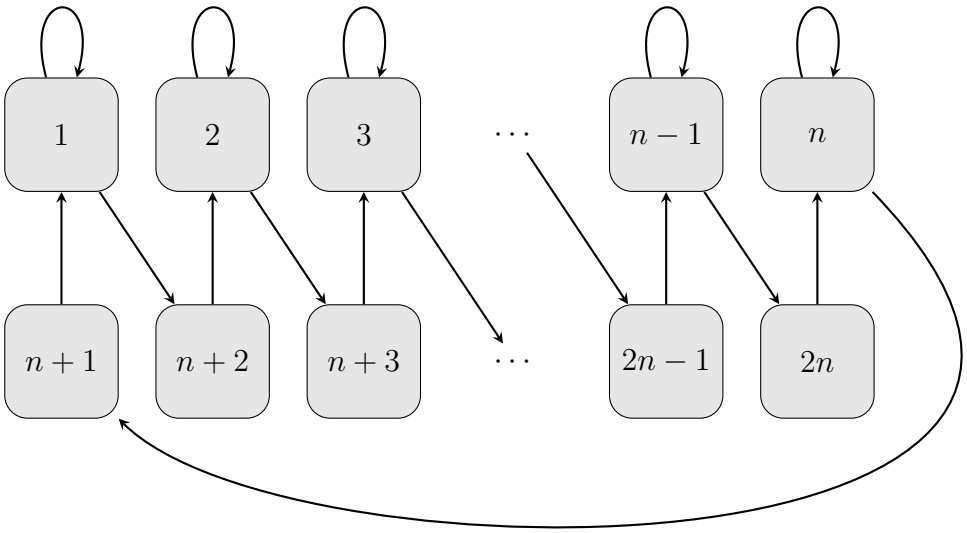

Thus we have a loop connecting all vertices, namely

$$n \to n+1 \to 1 \to n+2 \to 2 \to \cdots \to n-1 \to 2n \to n\,,$$

which ensures the strong connectivity. Furthermore, the loops of length 1 ensure the aperiodicity. We may therefore again apply the Perron-Frobenius theorem, although most of its statements follow already directly from our explicit computation of the eigenvalues. The main additional information is that the positive unit eigenvector to $\lambda_{0,+}$ determines the asymptotic distribution of the population over the different sizes. However, this eigenvector does not seem to possess a managable representation in closed form.

2.2 The Laney Model

In the model proposed by Laney, it is the larger daughter which needs more time until it can again reproduce. Here, this time lag is set to one generation. Compared to the Müller model, we must therefore swap the matrices A_0 and A_1 leading to the second-order difference system

$$x(t+1) = pA_1x(t) + \beta p^2 A_0 x(t-1)\,.$$

Thus the propagation matrix is now given by

$$P_{2n} = \begin{pmatrix} pA_1 & \beta^2 p^2 I_n \\ I_n & 0 \end{pmatrix} .$$

We use now a variant of the trick applied to the Müller model to compute the characteristic polynomial χ_{2n} of P_{2n}. Assuming this time that the matrix D is invertible, we can write

$$\begin{pmatrix} A & B \\ C & D \end{pmatrix} \begin{pmatrix} I & 0 \\ -D^{-1}C & I \end{pmatrix} = \begin{pmatrix} A - BD^1C & B \\ 0 & D \end{pmatrix}$$

and obtain now instead of (12)

$$\det \begin{pmatrix} A & B \\ C & D \end{pmatrix} = \det \left(A - BD^{-1}C\right) \det D \, . \tag{13}$$

Thus we find that

$$\chi_{2n}(\lambda) = \det \left(-\lambda I_n\right) \det \left(pA_1 - \left(\lambda + \frac{\beta^2 p^2}{\lambda}\right) I_n \right) .$$

It follows now from (2) that

$$\chi_{2n}(\lambda) = (\lambda^2 - \beta^2 p^2)^n - (p\sigma)^n \lambda^n \, .$$

Because of the very special form of this polynomial, it is straightforward to determine the eigenvalues:

$$\lambda_{i,\pm} = -\frac{\zeta_i^{(n)} p\sigma}{2} \pm \sqrt{\left(\frac{\zeta_i^{(n)} p\sigma}{2}\right)^2 + \beta^2 p^2} \, . \tag{14}$$

Thus all eigenvalues are simple. Real eigenvalues are obtained for $i = 1$ (as $\zeta_1^{(n)} = 1$) and for even n additionally for $i = n/2$ (as then $\zeta_{n/2}^{(n)} = -1$).

Again the propagation matrix P_{2n} is nonnegative and irreducible. The associated direct graph G_{2n} has the following form:

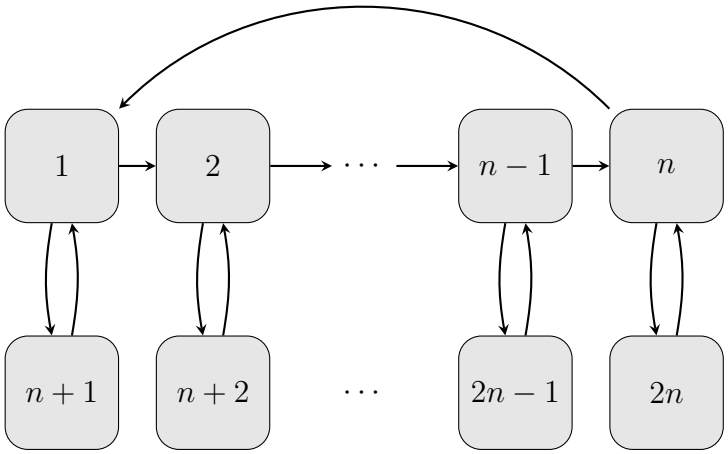

A path going through all vertices is given by

$$1 \to n+1 \to 1 \to 2 \to n+2 \to 2 \to 3 \to \cdots \to n \to 2n \to n \to 1\,,$$

hence G_{2n} is strongly connected. It has length $3n$ and a loop of length 2 is given by $1 \to n+1 \to 1$. In addition, there are loops of any length $n+2k$ for $0 \le k < n$ obtained by augmenting the loop $1 \to 2 \to \cdots \to n \to 1$ by k "detours" $\ell \to n+\ell \to \ell$. If n is odd, this observation implies that the matrix is aperiodic. For even n, the period of G_{2n} is 2.

The dominant eigenvalues can be obtained from (14). For odd n, the single dominant eigenvalue is

$$\lambda_{1+} \approx \frac{\beta^2 p}{\sigma}\,.$$

For even n the positive dominant eigenvalue is

$$\lambda_{n/2,+} \approx p\sigma + \frac{\beta^2 p}{\sigma}$$

and thus larger. The second dominant eigenvalue is in this case also real, namely $\lambda_{1-} = -\lambda_{n/2,+}$ (note that $q_1 = -q_{n/2} < 0$) and causes oscillations with a period of 2 generations as observed in the simulations. Since for nonnegative initial vectors negative populations will never result, the eigenvector with negative eigenvalue cannot occur alone, but is possibly mixed to the positive dominant eigenvector.

3 Models with Age Structure

3.1 Pristine initial cells

We consider now a linear model where the age of the diatoms is taken into account. We restrict to the case where the auxospores lead to pristine cells and assume that there are n size classes and m age classes. We denote by $X_{i,j}^{(n,m)}$ the number of diatoms in size class i and in age class j and interpret these values as entries of an $n \times m$ matrix $X^{(n,m)}$. Recall that we number the size classes by $0, 1, \ldots, n-1$ (with 0 denoting the largest size) and the age classes by $0, 1, \ldots, m-1$ (with 0 denoting the cells newly generated from auxospores) and we use the same indexing scheme for this matrix.

The model is then described by the following difference equations where special cases appear at the lower and left boundary of the matrix $X^{(n,m)}$. In the generic case where $i \neq n-1$ and $j \neq 0$ we have

$$X_{i,j}^{(n,m)}(t+1) = \beta p X_{i,j-1}^{(n,m)}(t) + p X_{i+1,j}^{(n,m)}(t)\,. \tag{15a}$$

At the bottom of the matrix we get for $j \neq 0$

$$X_{n-1,j}^{(n,m)}(t+1) = \beta p X_{n-1,j-1}^{(n,m)}(t) \tag{15b}$$

and at the left side of the matrix for $i \neq n-1$

$$X_{i,0}^{(n,m)}(t+1) = p X_{i+1,0}^{(n,m)}(t)\,. \tag{15c}$$

Finally, the generation of new cells from auxospores leads to

$$X_{n-1,0}^{(n,m)}(t+1) = s \sum_{j=0}^{m-1} X_{0,j}^{(n,m)}(t)\,. \tag{15d}$$

For expressing all these linear difference equations in the standard form of a matrix difference equation $X^{(n,m)}(t+1) = P^{(n,m)} X^{(n,m)}(t)$ with an $nm \times nm$ matrix $P^{(n,m)}$, we rewrite the matrix $X^{(n,m)}$ as an nm-dimensional vector – which we continue to denote by $X^{(n,m)}$ – by stacking the columns, i. e. the transpose of the vector $X^{(n,m)}$ is given by

$$(X_{0,0}^{(n,m)}, \ldots, X_{n-1,0}^{(n,m)}, X_{0,1}^{(n,m)}, \ldots, X_{n-1,1}^{(n,m)}, \ldots, X_{0,m-1}^{(n,m)}, \ldots, X_{n-1,m-1}^{(n,m)})\,.$$

We will write the propagation matrix $P^{(n,m)}$ as an $m \times m$ block matrix with blocks which are $n \times n$ matrices. For this purpose, we introduce the following three $n \times n$ matrices:

$$D_n = \begin{pmatrix} 0 & 1 & 0 & \cdots & 0 \\ & \ddots & \ddots & \ddots & \vdots \\ & & \ddots & \ddots & 0 \\ & & & \ddots & 1 \\ 0 & & & & 0 \end{pmatrix} , \quad S_n = \begin{pmatrix} 0 & \cdots & \cdots & 0 \\ \vdots & & & \vdots \\ 0 & & & \vdots \\ \sigma^n & 0 & \cdots & 0 \end{pmatrix} , \quad B_n = \beta I_n ,$$

where as before $s = \sigma^n p$. Now we can write $P^{(n,m)} = pA^{(n,m)}$ with

$$A^{(n,m)} = \begin{pmatrix} D_n + S_n & S_n & \cdots & S_n \\ B_n & D_n & & 0 \\ & \ddots & \ddots & \\ 0 & & B_n & D_n \end{pmatrix} . \tag{16}$$

As in the previous sections, our first task consists of computing the characteristic polynomial $\chi^{(n,m)}(\mu) = \det(A^{(n,m)} - \mu I_{nm})$. If we abbreviate $\hat{D}_n = D_n - \mu I_n$, then we can write

$$A^{(n,m)} - \mu I_{nm} = \begin{pmatrix} \hat{D}_n + S_n & \tilde{S}_n \\ \tilde{B}_n & \tilde{D}_{n,m-1} \end{pmatrix} \tag{17}$$

where $\tilde{S}_n$ is the $n \times n(m-1)$ matrix $(S_n \ \cdots \ S_n)$ with $m-1$ blocks and where the matrices

$$\tilde{B}_n = \begin{pmatrix} B_n \\ 0 \\ \vdots \\ 0 \end{pmatrix} , \qquad \tilde{D}_{n,m-1} = \begin{pmatrix} \hat{D}_n & & & 0 \\ B_n & \hat{D}_n & & \\ & \ddots & \ddots & \\ 0 & & B_n & \hat{D}_n \end{pmatrix}$$

have $m-1$ block rows. We first note that the matrix $\hat{D}_n$ is invertible (over the field $\mathbb{R}(\mu)$ of rational functions in μ) with inverse

$$\hat{D}_n^{-1} = -\begin{pmatrix} \mu^{-1} & \mu^{-2} & \cdots & \mu^{-n} \\ & \ddots & \ddots & \vdots \\ & & \ddots & \mu^{-2} \\ & & & \mu^{-1} \end{pmatrix} , \tag{18}$$

as one can easily verify. For later use, we note that also the powers of this inverse possess a simple closed form representation: for any integer $k > 0$ we find the following upper triangular matrix

$$\hat{D}_n^{-k} = (-1)^k \begin{pmatrix} \binom{k-1}{k-1}\mu^{-k} & \binom{k}{k-1}\mu^{-k+1} & \cdots & \binom{k+n-2}{k-1}\mu^{-k-n+1} \\ & \ddots & \ddots & \vdots \\ & & \ddots & \binom{k}{k-1}\mu^{-k+1} \\ & & & \binom{k-1}{k-1}\mu^{-k} \end{pmatrix} . \tag{19}$$

This can be easily shown by repeated multiplication with $\hat{D}_n^{-1}$ and by noting that the arising numerical coefficients represent a column sum in Pascal's triangle, i. e. by using the identity

$$\sum_{j=0}^{\ell} \binom{j}{i} = \binom{\ell+1}{i+1} . \tag{20}$$

As a consequence of the above observation, the matrix $\tilde{D}_{n,m-1}$ is invertible, too. It is straightforward to verify that its inverse is given by

$$\tilde{D}_{n,m-1}^{-1} = \begin{pmatrix} \hat{D}_n^{-1} & & & 0 \\ -\beta\hat{D}_n^{-2} & \hat{D}_n^{-1} & & \\ & \ddots & \ddots & \\ (-\beta)^{m-1}\hat{D}_n^{-m} & \cdots & -\beta\hat{D}_n^{-2} & \hat{D}_n^{-1} \end{pmatrix}$$

Here we exploited that B_n is a multiple of an identity matrix and hence multiplication by it corresponds to a scalar multiplication with β.

After these preparations, we apply (13) to (16) and obtain

$$\chi^{(n,m)}(\mu) = \det\left(\hat{D}_n + S_n - \tilde{S}_n\tilde{D}_{n,m-1}^{-1}\tilde{B}_n\right) \cdot \det\left(\tilde{D}_{n,m-1}\right) . \tag{21}$$

As $\tilde{D}_{n,m-1}$ possesses a block triangular form with triangular blocks $\hat{D}_n$ on the diagonal, it follows immediately that the last determinant is given by

$$\det\left(\tilde{D}_{n,m-1}\right) = \det\left(\hat{D}_n\right)^{m-1} = (-\mu)^{n(m-1)} .$$

The form of the matrices $\tilde{S}_n$ and $\tilde{B}_n$ and the above determined expression for the inverse $\tilde{D}^{-1}_{n,m-1}$ yield in a straightforward computation that

$$\tilde{S}_n \tilde{D}^{-1}_{n,m-1} \tilde{B}_n = \sum_{k=1}^{m-1} (-\beta)^k S_n \hat{D}_n^{-k} \,.$$

The product $S_n \hat{D}_n^{-k}$ yields a matrix where all rows are zero except of the bottom one which is σ^n times the top row of $\hat{D}_n^{-k}$. Thus the product $\tilde{S}_n \tilde{D}^{-1}_{n,m-1} \tilde{B}_n$ leads also to an $n \times n$ matrix where only the bottom row contains non-zero entries. If we denote the jth entry of the bottom row by b_j, then

$$b_j = \sum_{k=1}^{m-1} \binom{k+j-2}{k-1} \sigma^n \beta^k \mu^{-k-j-1} \,.$$

Now we can write out the remaining determinant explicitly:

$$\det\left(\hat{D}_n + S_n - \tilde{S}_n \tilde{D}^{-1}_{n,m-1} \tilde{B}_n\right) = \begin{vmatrix} -\mu & 1 & & & 0 \\ & -\mu & 1 & & \\ & & \ddots & \ddots & \\ 0 & & & -\mu & 1 \\ b_1 + \sigma^n & b_2 & \cdots & b_{n-1} & b_n - \mu \end{vmatrix} .$$

We expand this determinant along the bottom row, as the thereby arising determinants are trivial to compute. Furthermore, we treat the summands σ^n and $-\mu$, respectively, in the first and the last entry of the bottom row separately. This procedure yields

$$\begin{aligned} &\det\left(\hat{D}_n + S_n - \tilde{S}_n \tilde{D}^{-1}_{n,m-1} \tilde{B}_n\right) = \\ &\qquad (-\mu)^n + (-1)^{n+1}\sigma^n + \sum_{j=1}^{n} \sum_{k=1}^{m-1} (-1)^{n+j} \binom{k+j-2}{k-1} \sigma^n \beta^k \mu^{-k} = \\ &\qquad\qquad (-1)^n \left[\mu^n - \sigma^n \sum_{k=1}^{m-1} \binom{k+n-1}{k} \beta^k \mu^{-k} \right] \end{aligned}$$

where in the last equality we have used again the formula (20) for column sums in Pascal's triangle. Putting everything together, we arrive at the following expression for the characteristic polynomial:

$$\chi^{(m,n)}(\mu) = (-1)^{nm} \left[\mu^{mn} - \sigma^n \sum_{k=0}^{m-1} \binom{k+n-1}{k} \beta^k \mu^{(m-1)n-k} \right] . \qquad (22)$$

The eigenvalues of the propagation matrix $P^{(n,m)}$ are given by p times the zeros of the polynomial $\chi^{(n,m)}(\mu)$. A first immediate observation is that 0 is an $(n-1)(m-1)$-fold eigenvalue of $P^{(m,n)}$. Since σ and β are positive parameters, the coefficients of the characteristic polynomial $\chi^{(m,n)}(\mu)$ show only one sign change. Hence, by Descartes' rule of signs[3] there exists exactly one positive root (counted with multiplicity). One can easily derive a necessary and sufficient condition for $1/p$ to be this unique positive root (meaning that 1 is an eigenvalue of $P^{(n,m)}$):

$$s = p\sigma^n = \frac{p}{\sum_{k=0}^{m-1} \binom{k+n-1}{k} \beta^k p^{n+k}} \; . \tag{23}$$

The polynomial $\chi^{(m,n)}(-\mu)$ exhibits m sign changes in the coefficients except in the case that m is even and n is odd. In that case we have only $m-2$ sign changes. In any case, by Descartes' rule, we can have at most m negative eigenvalues (again counted with multiplicities). Thus our matrix possesses at most $nm - n + 2$ real eigenvalues which implies that for $n > 2$ also complex eigenvalues must exist.

Using Gershgorin's circle theorem[4], one can deduce furthermore that all eigenvalues lie in a disc centred at the origin of the complex plane with a radius r given by

$$r = \max\left\{p,\ \min\left\{m\sigma^n, 1\right\},\ \min\left\{s, p\beta\right\}\right\} \; . \tag{24}$$

This follows immediately from the fact that all diagonal elements in the propagation matrix $P^{(n,m)}$ vanish and that for each index i the minimum of the sum of the non-diagonal elements of either row i or column i is given by one of the above expressions.

For applying the Perron-Frobenius theorem, we must again verify first that the matrix $P^{(n,m)}$ is irreducible. Thus we look at the associated directed graph $G^{(n,m)}$ which has the following structure:

[3] See e. g. Henrici P. 1974 Applied and Computational Complex Analysis, Vol. 1, Wiley (Thm. 6.2d).

[4] Ibid. (Thm. 7.8d)

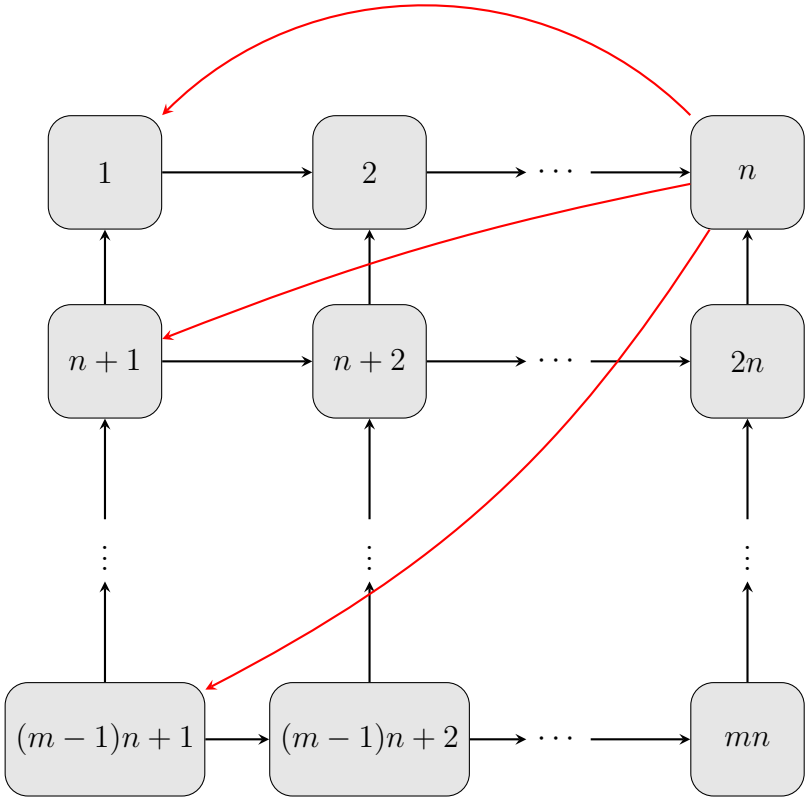

The red arrows correspond to the edges determined by the auxosporulation. They all start at the same vertex because of our assumption that auxospores always generate pristine cells and they are crucial for the strong connectivity of the graph $G^{(n,m)}$. A path going through all vertices (visiting some several times) can be given as follows:

$$\begin{aligned} &1 \to 2 \to \cdots \to n \to n+1 \to n+2 \to \cdots \to 2n \to n \to \\ &2n+1 \to 2n+2 \to \cdots \to 3n \to 2n \to n \to 3n+1 \to \cdots \to \\ &4n \to \cdots \to n \to 4n+1 \to \cdots \to mn \to (m-1)n \to \cdots \to n \to 1\ . \end{aligned}$$

A loop of length n is given by $1 \to 2 \to \cdots \to n \to 1$. A loop of length $n+1$ can be constructed by prepending $n+1$: $n+1 \to 1 \to 2 \to \cdots \to n \to n+1$. This implies that the greatest common divisor of the loop lengths can only be 1 and our matrix is also aperiodic.

Thus all conditions of the Perron-Frobenius theorem are satisfied and we can conclude that our matrix possesses a unique dominant eigenvalue which

is given by the single positive real root of the characteristic polynomial. Furthermore, we know from the above application of Gershgorin's circle theorem that a bound r for this root is given by (24). Because of our assumptions on the parameters p, β and s, we obviously have that $r \leq 1$.

Finally, we analyse in more detail what happens for the special initial condition $X_{n-1,0}(0) = 1$ and $X_{i,j}(0) = 0$ for all other values of (i, j), i. e. for an initial population of one pristine cell of maximal size. It follows from (15) that such cells can only be generated via auxospores and cells of any other combination of size and age only via cell division. The number $X_{i,j}(t)$ of cells obtained via cell division in generation t can be easily determined using again Pascal's triangle. After $n + m - 1$ generations all cells obtained this way have disappeared. In the tth generation with $0 < t < n + m$, we have $X_{i,j}(t) = \beta^j p^t \binom{t}{j}$ for $n - 1 - i + j = t$ (and of course $i < n$, $j < m$) and $X_{i,j}(t) = 0$ else. Thus the initial "seed" in the lower left corner of the matrix moves like a wavefront through the matrix X with always all non-vanishing entries in one diagonal.

If we assume that $n > m$, then the first auxospore formation happens in generation n: $X_{n-1,0}(n) = X_{0,0}(n-1) = 1$. In the following generations we obtain $X_{n-1,0}(n+k) = X_{0,k}(n+k-1) = \beta^k p^{n+k-1} \binom{n+k-1}{k}$ for $0 \leq k < m$. For the special case $\beta = p = 1$, the total number of auxospores having their origin in our "seed" can be determined via a well-known identity for binomial coefficients:

$$\sum_{j=0}^{m-1} \binom{n-1+j}{j} = \binom{n+m-1}{m-1}.$$

3.2 Initial cells with age memory

So far, we assumed that any cell generated by auxospores is pristine. We now look at the hypothetical possibility that auxospores retain the age of the cells from which they stem. In this case, we must replace $A^{(n,m)}$ by the matrix

$$\bar{A}^{(n,m)} = \begin{pmatrix} D_n + S_n & & & 0 \\ B_n & D_n + S_n & & \\ & \ddots & \ddots & \\ 0 & & B_n & D_n + S_n \end{pmatrix}.$$

The directed graph $\bar{G}^{(n,m)}$ associated with it has the following form:

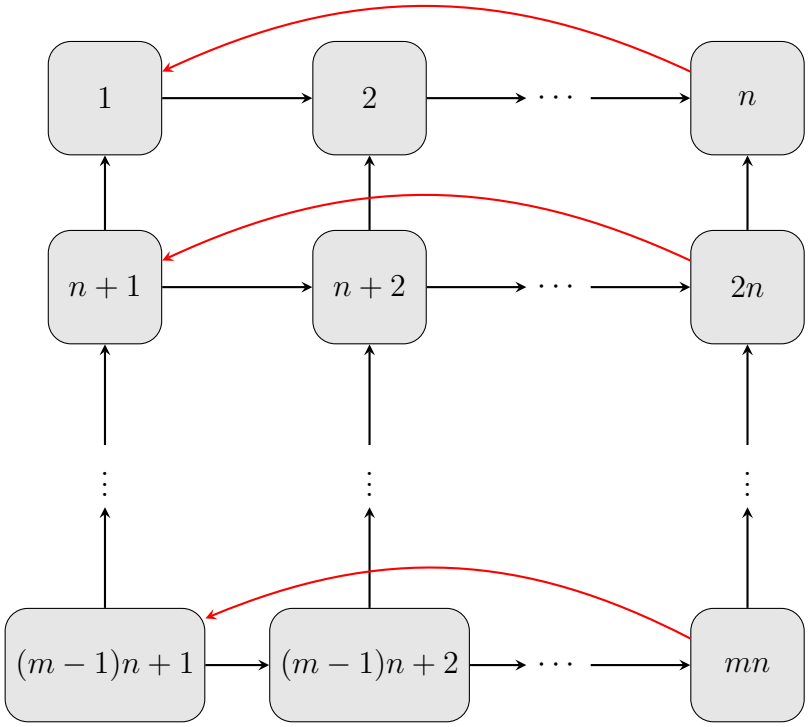

Compared to the model in the previous section, only the red edges have changed. Because of this change, the propagation matrix is no longer irreducible. Indeed, one can easily see that the vertices $(m-1)n+1, \ldots, mn$ form a subgraph in form of a loop into which no edge from the remaining graph points. Hence it is not possible to reach these vertices from the rest of the graph. Thus the Perron-Frobenius theorem cannot be applied and cyclic oscillations as dominant modes may indeed occur, as observed in the simulations. Even if the biological reality is questionable, this model variant is an instructive counterexample to the idea that all linear models only lead to decaying oscillations.

4 Special Algorithms

Algorithms and simulation results for special models that require a modification of the basic algorithm (Supplemental Information 5) are explained here. Only the key lines are given, header and output modules are the same as in the full model in Supplemental Information 5.

a) Size dependent cell division probability

Here it is assumed that the proliferation probability drops continuously from larger cells to smaller cells. Since the *roll* function of the *numpy* library cannot used be conveniently, the size classes were treated consecutively in a loop instead of the algorithm of Supplementary Information 5.
Here, the proliferation probability was linearly varied from nominally $p/2$ for the smallest size to p for the largest size. α was set to zero, though, and auxosporulation probability to s. Nutrient saturation and ageing was not applied.

Key algorithm:

```
p = 0.68 #maximum proliferation probability
dp=0 #for basic linear model
dp =0.5*p/(numsizes-1) #change of p with size
sigma = 1 # relative probability for auxospore formation
s=p*sigma**numsizes
beta = 1 #asymmetry between half cells
cells=np.zeros(numsizes)

""" Main loop """
cells[numsizes-1]=1   #initial cell
for gen in range (numgen+1):
    auxospores=s*cells[0]
    cells[0]=0        #alpha=0
    for i in range(numsizes-1):
        p_i=p-dp*(numsizes-1-i)
        cells[i]=beta*cells[i]+cells[i+1]
        cells[i]*=p_i
    cells[-1]*=p
    cells[-1]+=auxospores
    for i in range(numsizes):
         number[gen]+=cells[i]
         mom1[gen]+=cells[i]*i
         mom2[gen]+=cells[i]*i*i
    mom1[gen]=mom1[gen]/number[gen]
    mom2[gen]=mom2[gen]/number[gen]
    var[gen]=mom2[gen]-mom1[gen]**2
    auxo[gen]=auxospores
```

Example output:

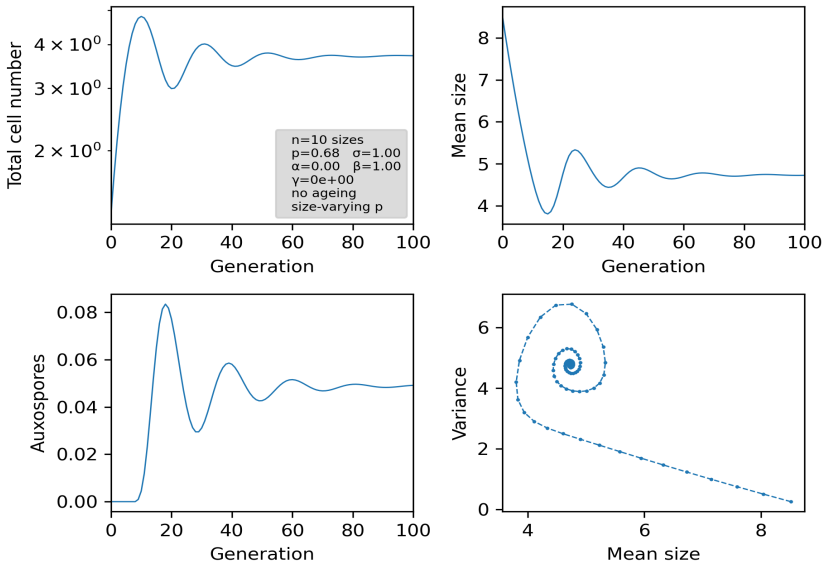

Decaying oscillations similar to results with a constant mean value of *p* are observed.

b) Müller delay model

Here, the smaller daughter is subjected to a delay of one generation until it can reproduce vegetatively or undergo auxosporulation.

Modified algorithm:

```
cw=np.zeros(numsizes) #resting cells
cells[numsizes-1]=1 #initial cell
for gen in range (numgen+1):
    for i in range(numsizes):
         number[gen]+=cells[i]+cw[i] #other outputs accordingly
    auxospores=s*cells[0]
    for i in range (numsizes-1):
        h=cells[i+1]      #smaller daughters
        cells[i]+=cw[i]   #back from resting phase
        cw[i]=h*p         #smaller daughters in resting phase
        cells[i]*=beta*p #here alpha=beta
    cells[-1]+=cw[-1]
    cw[-1]=auxospores
    cells[-1]*=beta*p
    auxo[gen]=auxospores
```

Example output:

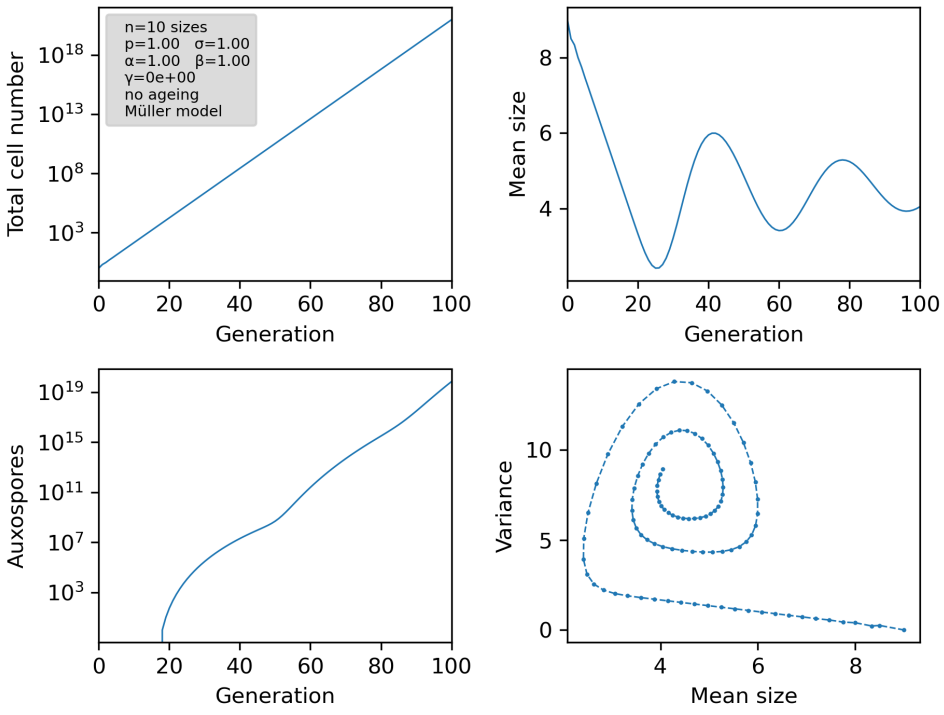

Decaying oscillations with longer periods are observed.

c) Laney delay model

Here, the larger daughter is subjected to a delay of one generation until it can reproduce vegetatively. Auxosporulation is spontaneous according to presettings, but may be set manually to a delay.

Modified algorithm:

```
cw=np.zeros(numsizes) #resting cells
cells[numsizes-1]=1 #initial cell
for gen in range (numgen+1):
    for i in range(numsizes):
         number[gen]+=cells[i]+cw[i] #other outputs accordingly
    auxospores=s*cells[0]
    for i in range(numsizes):
        cells[i],cw[i]=p*cw[i],p*cells[i] # flip to/from resting phase
    for i in range (numsizes-1):
        cells[i]+=cw[i+1] #smaller daughter
        cw[i]*=beta       #here alpha=beta
    cw[-1]*=beta
#    cw[-1]+=auxospores  #if auxospores are delayed
    cells[-1]+=auxospores #if auxospores are not delayed
    auxo[gen]=auxospores
```

Example output:

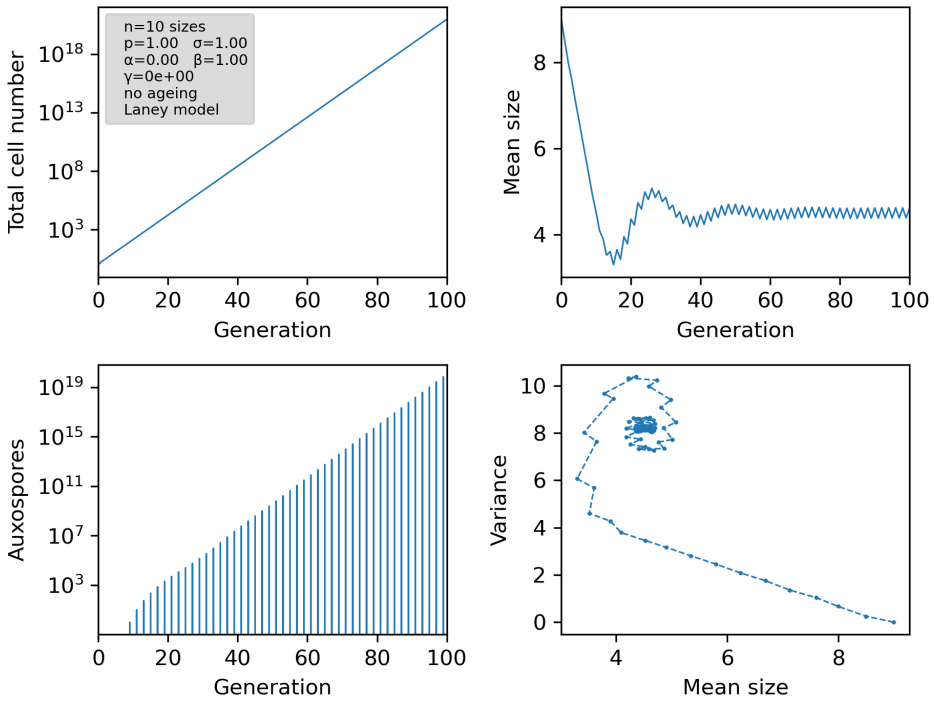

High-frequency oscillations with a period of 2 generations and small amplitudes have been observed.

d) Biparental sexual phase

Here, the auxosporulation probability depends on the cell density as in a bimolecular chemical reaction, with saturation per generation due to the limited number of gametes.

In the algorithm from a) the expression

```
auxospores=s*cells[0]
```

was replaced by

```
auxospores=s*cells[0]*cells[0]/(1+2*s*cells[0])
```

For size-invariant *p* (`dp=0`), typical results are as in the following output for *p*=0.56

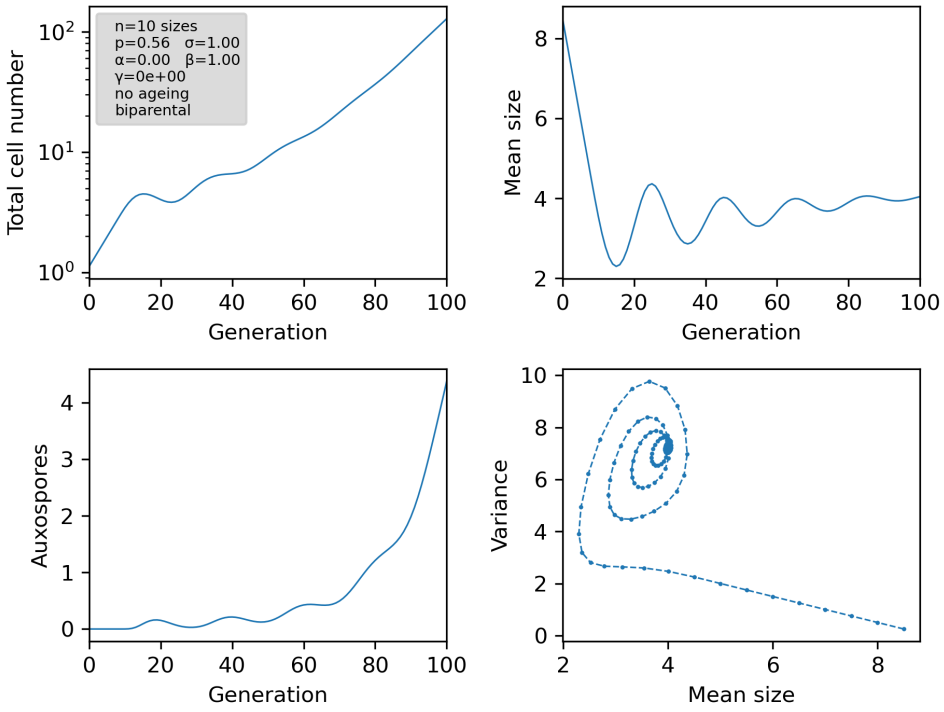

The nonlinearity causes a shift of the equilibrium during the relaxation of the oscillations, but sustained oscillations have not been found.

5 Python Source Code

```
# -*- coding: utf-8 -*-
"""
Diatom population simulation with size and age structure
Program written by T.Fuhrmann-Lieker and N. Kubetschek
"""

"""used packages"""
import numpy as np
import matplotlib.pyplot as plt
from scipy.signal import  find_peaks, peak_widths
from scipy import signal
import scipy.optimize as opt
import matplotlib as mpl
from scipy.stats import betabinom
mpl.rcParams['agg.path.chunksize'] = 100000


""" Model definition """
numsizes = 50 # number of different cell sizes, smallest has index zero
p = 1 #proliferation probability
sigma_n = 1 # relative probability for auxospore formation
beta = 1 #asymmetry between half cells
alpha = 1 # first diagonal element


""" Nonlinearity """
gamma = 1e-3 #in Ricker model, set to zero for linear model
# for other nonlinear models see below

""" Ageing """
ageing = 1 #0: no ageing 1:ageing
lifespan = 5 #m
if ageing==0: lifespan = 1 #lifespan has no effect without ageing
juvenile = True # age of new cells reset to zero

""" Run parameters """
numgen = 100000 #100000*(numsizes+lifespan-1) # number of generations
every = numgen/5 #output every n generation

""" Output file """
filename=("sigma=1,n=50,m=5_")
paramsfile=filename+'param.txt'
paramsfitfile=filename+"Weibull_param.txt"
paramsfitfiledis=filename+"betabinom_param.txt"
param=filename+"inversebetabinom.txt"
paramstable=filename+"table.txt"
graphsfile1=filename+'1.png'
graphsfile2=filename+'2.png'
graphsfile3=filename+'3.png'
graphsfile4=filename+'4.png'
graphsfile5=filename+'5.png'
graphsfile6=filename+'6.png'
graphsfile7=filename+'7.png'
graphsfile8=filename+'8.png'
graphsfile9=filename+'9.png'
graphsfile10=filename+'10.png'

""" Plot parameters """
font = {'family' : 'sans-serif',
        'weight' : 'normal',
        'size'   : 10}
```

```
""" Predefinitions """
cells=np.zeros((numsizes,lifespan)) #histogram array coding size and age
agedcells=np.zeros((numsizes,lifespan)) #represents ageing of actual cells
newcells=np.zeros((numsizes,lifespan))#represents new cells without ageing
distribution=np.zeros(numsizes) #histogram size only
u=np.ones(lifespan) #help array for contracting cells to distribution
size=np.arange(numsizes) #integer array for computing statistics
size2=size*size #squared integer array for computing statistics
size3=size*size2 #cubed integer array
number=np.zeros(numgen+1) #output array cell total number
mom1=np.zeros(numgen+1) #output array average size
mom2=np.zeros(numgen+1) #output array second moment of distribution
var=np.zeros(numgen+1) #output array variance of distribution
auxo=np.zeros(numgen+1) #output array auxospores

cells[numsizes-1,0] = 1 #initial condition: one cell of largest size, pristine
load = 0

""" Log file """
if (ageing==1):
    txt='with ageing (m={0:d})'.format(lifespan)
else:
    txt='no ageing'
if (juvenile==True):
    txt = txt+'\nnew cells juvenile'
legendtext = 'n={0:d} sizes\np={1:.2f}   \u03c3={2:.2f}\n\u03b1={3:.2f}   \
\u03b2={4:.2f}\n\u03b3={5:.0e}\n{6:s}'\
    .format(numsizes,p,sigma_n,alpha,beta,gamma,txt)
stream=open(paramsfile,'w',encoding='utf-8')
stream.write(legendtext)
stream.close()
#p=p*np.arange(1.0,0.0,-1/numsizes) #for size-dependent p

""" Main Loop """
for gen in range (numgen+1): #loop for generations
    if (gen)%every==0: #output not for every step
        plt.figure(figsize=(3.3,2.6),dpi=300)
        plt.rc('font', **font) #formatting for plots
        plt.plot(cells.dot(u),"ob--",markersize=4,label=legendtext)
        plt.title('after {0:d} generations'.format(gen),size=10)
        plt.xlim(0,numsizes-1)
        plt.xlabel('Cell size index')
        plt.xticks(np.arange(0,numsizes,numsizes/10))
        plt.xticks(rotation=45)
        plt.ylabel('Number of cells')
        plt.legend(loc='best',fontsize='x-small',handlelength=0,
             markerscale=0,facecolor='lightgrey')
        plt.tight_layout()
        plt.savefig("sigma=1,n=50,m=5_generation{0:3d}.png".format(gen),\
                    dpi=300)
        plt.show()

#    p=0.75+0.25*(np.cos(np.pi*gen/20))**2 #zeitgeber
    distribution=cells.dot(u) #calculating size distribution
    number[gen]=np.sum(distribution) #calculating total number
    mom1[gen]=np.sum(size*distribution)/number[gen] #calculating 1st moment
    mom2[gen]=np.sum(size2*distribution)/number[gen] #calculating 2nd moment
    var[gen]=mom2[gen]-mom1[gen]**2 #calculating variance
    load=number[gen] #or mom1[gen]*number[gen] etc.
    agedcells=np.roll(cells,ageing,axis=1)
    agedcellsT=agedcells.transpose()
    agedcellsP=p*agedcellsT
    agedcells=agedcellsP.transpose()
```

```
        #shift array to right for ageing
    if (ageing==1): agedcells[:,0]=0 #reentered old cells removed
    agedcells[0,:]*=alpha #correction for smallest size
    agedcells[1:,:]*=beta
    newcells=np.roll(cells,-1,axis=0) #shift upwards for new smaller cells
    newcellsT=newcells.transpose()
    newcellsP=p*newcellsT
    newcells=newcellsP.transpose()
    newcells[-1,:]*=sigma_n**numsizes

    if (juvenile==True): #auxospore zero age
        newcells[-1,0]=np.sum(newcells[-1,:])
        newcells[-1,1:]=0

    auxo[gen]=np.sum(newcells[-1,:])

    # formation of next generation:
    cells=(agedcells+newcells)*np.exp(-gamma*load) #Ricker
#    cells=(agedcells+newcells)/((1+gamma*(load))**2) #Hassell


""" Output plots """

plt.figure(figsize=(6.3,4.8),dpi=300)
plt.rc('font', **font) #formatting for plots
plt.subplot(2,2,1)
plt.plot(number,linewidth=0.75,label=legendtext)
plt.ylabel('Total cell number')
plt.yscale('log')
plt.xlim(0,numgen)
plt.xlabel('Generation')
plt.xticks(rotation=45)
plt.legend(loc='best',fontsize='x-small',handlelength=0,
     facecolor='lightgrey')
plt.tight_layout()

plt.subplot(2,2,2)
plt.plot(mom1,linewidth=0.75)
plt.ylabel('Mean size')
plt.yscale('linear')
plt.xlim(0,numgen)
plt.xlabel('Generation')
plt.xticks(rotation=45)
plt.tight_layout()

plt.subplot(2,2,3)
plt.plot(auxo,linewidth=0.75)
plt.ylabel('Auxospores')
plt.xlim(0,numgen)
plt.xlabel('Generation')
plt.xticks(rotation=45)
plt.tight_layout()

plt.subplot(2,2,4)
plt.plot(mom1,var,'o--',markersize=1,linewidth=0.75)
plt.ylabel('Variance')
plt.xlabel('Mean size')
plt.xticks(rotation=45)
plt.tight_layout()
plt.savefig(graphsfile1)
plt.show()

mn=np.mean(number)
```

```
xi=np.linspace(0, 1.0, numgen+1, endpoint=True)
z=np.fft.fft(number-mn)/(numgen+1)
zpow=np.absolute(z)**2
acf=np.fft.ifft(zpow)

#print('Peaks in population \n', signal.find_peaks(number)[0])
popks=signal.find_peaks(number)[0]  #find t-value maxima of cell size
dumarray=[]
for peak in popks:
    "print(peak,number[peak])"
    dumarray.append(number[peak])
popksheight=np.array(dumarray) #y-value of cell size maxima
print('Peaks in mean size: \n', signal.find_peaks(mom1)[0])
print('Peaks in auxospores: \n',signal.find_peaks(auxo)[0])
print('Peaks in variance: \n',signal.find_peaks(var)[0])
print('Freq\tPeriod')
pks=signal.find_peaks(zpow,height=0.005)[0]
for freq in pks:
    print('{0:.4f}\t{1:.2f}'.format(xi[freq],1/xi[freq]))
print('Peaks in acf: \n',signal.find_peaks(acf)[0])

popks_m=signal.find_peaks(number*-1)[0] #find t-value of cell size minima
dumarray_m=[]
for peak_m in popks_m:
    dumarray_m.append(number[peak_m])
popksheight_m=np.array(dumarray_m)

plt.figure(figsize=(6.3,4.8),dpi=300)
plt.rc('font', **font) #formatting for plots
plt.subplot(2,2,1)
plt.plot(xi,zpow,linewidth=2,color='r')
plt.xlim(0,5/numsizes)
plt.tick_params(axis='both',width=2)
plt.plot(xi[pks],zpow[pks],"x")
plt.ylabel('Power spectrum')
plt.xlabel('Frequency')
plt.tight_layout()

plt.subplot(2,2,2)
plt.plot(acf/acf[0],linewidth=1.5,color='b')
plt.xlim(0,numgen/4)
plt.tick_params(axis='both',width=2)
plt.ylabel('ACF')
plt.xlabel('Generation')
plt.xticks(rotation=45)
plt.tight_layout()

plt.subplot(2,2,3)
plt.plot(var,linewidth=0.75)
plt.ylabel('Variance')
plt.xlim(0,numgen)
plt.xlabel('Generation')
plt.xticks(rotation=45)
plt.tight_layout()

plt.subplot(2,2,4)
plt.plot(popks,popksheight,'o--',markersize=1,linewidth=0.75)
plt.ylabel('Population peak')
plt.xlabel('Generation')
plt.xticks(rotation=45)
plt.tight_layout()
plt.savefig(graphsfile2)
plt.show()
```

```
"""fitting weibull distribution on maxima and minima"""

"""fitting population peak maxima vs. generation with weibull distribution:"""
t = popks[popks>(numsizes+lifespan+50)]
y = popksheight[popks>(numsizes+lifespan+50)]
def f(t,A1,A2,tau,c):
    return A2+(A1-A2)*np.exp(-(t/tau)**c)
(A1_,A2_,tau_,c_), _max = opt.curve_fit(f,t,y,p0=[700 , 400 , 13000 , 0.7])\
    #p0=Startparams for fitting
y_fit = f(t, A1_, A2_,tau_,c_)

"""fitting population peak minima vs. generation with weibull distribution:"""
t_m = popks_m[popks_m>20]
y_m = popksheight_m[popks_m>20]
def f_m(t_m,A1_m,A2_m,tau_m,c_m):
    return A2_m+(A1_m-A2_m)*np.exp(-(t_m/tau_m)**c_m)
(A1_m_,A2_m_,tau_m_,c_m_),_min=opt.curve_fit(f,t_m,y_m,p0=[180,400,22000,0.89])\
    #p0=startparams for fitting
y_m_fit = f(t_m, A1_m_, A2_m_,tau_m_,c_m_)

Fehler_max = np.sqrt(np.diag(_max))
Fehler_min = np.sqrt(np.diag(_min))
"""formatting Fit-parameters"""

legendt = 'n={0:d} sizes\nA1={1:.2f}           A2={2:.2f}\ntau={3:.2f} \
      c={4:.2f}\nA1_m={5:.2f}      A2_m={6:.2f}\ntau_m={7:.2f} \
          c_m={8:.2f}\n\n{9:s}'\
    .format(numsizes,A1_,A2_,tau_,c_,A1_m_,A2_m_,tau_m_,c_m_,txt)
stream=open(paramsfitfile,'w',encoding='utf-8')
stream.write(legendt)
stream.close()

"""plot data, fitted functions and tau"""
plt.figure(figsize=(6.3,4.8),dpi=300)
plt.rc('font', **font) #formatting for plots
plt.subplot(2,1,1)
plt.plot(number,linewidth=0.75,label=legendtext) #plot data
plt.ylabel('Total cell number')
plt.xscale("log")       #x-axis log
plt.xlabel('Generation')
plt.grid(True)
plt.xticks(rotation=45)

plt.axvline(x=tau_,color="red",linestyle="--") #plot tau for maxima fit
plt.axvline(x=tau_m_,color="green",linestyle="--") #plot tau for minima fit
plt.plot(t, y_fit,'r-') #plot fit to maxima
plt.plot(t_m,y_m_fit,'g-') #plot fit to minima
plt.legend(loc='best',fontsize='x-small',handlelength=0,
     facecolor='lightgrey')
plt.tight_layout()

"""plot maxima, minima and fits"""

plt.subplot(2,1,2)
plt.rc('font', **font) #formatting for plots
plt.plot(popks,popksheight,'o--',color="blue",markersize=0.5,linewidth=0.7,\
         label=legendt) #plot maxima data
plt.plot(popks_m,popksheight_m,"o--",color="blue",markersize=0.5,\
         linewidth=0.7) #plot minima data
plt.ylabel('Population peak')
plt.xlabel('Generation')
plt.xscale('log')
plt.grid(True)
plt.axvline(x=tau_,color="red",linestyle="--")  #plot maxima tau
```

```
plt.axvline(x=tau_m_,color="green",linestyle="--") #plot minima tau
plt.plot(t, y_fit,'r-')   #plot maxima fit
plt.plot(t_m,y_m_fit,'g')               #plot minima fit
plt.legend(loc='best',fontsize='x-small',handlelength=0,
     facecolor='lightgrey')
plt.tight_layout()
plt.savefig(graphsfile3) #save figure
plt.show()#plot figure

"""plot distribution"""
plt.figure(figsize=(3.3,2.6),dpi=300)
plt.rc('font', **font) #formatting for plots
plt.plot(size,distribution,"ob--",markersize=3,label=legendtext)
plt.title("Distribution",size=10)
plt.xlabel('cell size index')
plt.xticks(rotation=45)
plt.ylabel('Number of cells')
plt.savefig(graphsfile4)
plt.legend(loc='best',fontsize='x-small',handlelength=0,
     facecolor='lightgrey')
plt.show()

"""area standardized distribution with inverse x-axis"""
area = np.trapz(distribution,size) \
    #numeric integration, calculate area under distribution

#fit area standardized betabinominal fit with inverse x-axis
x=size*-1+(numsizes-1)
y=distribution/area
def f5(x,n,a,b,d11):
    return (1-d11)*betabinom.pmf(x,n,a,b)+d11
(n_,a_,b_,d11_),_dis=opt.curve_fit(f5,x,y,p0=[150.07,3.06,22.9,0.00011])
y_fit5=f5(x,n_,a_,b_,d11_)
Fehler_dis = np.sqrt(np.diag(_dis))
legendt_distribution ='n={0:d} sizes\na={1:.2f}      \nb={2:.2f}\nn_B={3:.2f} \
        \n{4:s}'\
    .format(numsizes,a_,b_,n_,txt)
stream=open(param,'w',encoding='utf-8')
stream.write(legendt_distribution)
stream.close()

#plot area standardized distribution with inverse x-axis and fit
plt.figure(figsize=(3.3,2.6),dpi=300)
plt.rc('font', **font) #formatting for plots
plt.plot(size*-1+(numsizes-1),distribution/area,"ob--",markersize=3,\
         label=legendt_distribution) #plot inverse distribution
plt.title("betabinominal, inverse x-Axis",size=10)
plt.xlabel('inverse cell size index')
plt.xticks(rotation=45)
plt.ylabel('Number of cells/area')
plt.plot(x,y_fit5,"g-",label="betabinominal")
plt.legend(loc='best',fontsize='x-small',handlelength=0,
     facecolor='lightgrey')
plt.savefig(graphsfile5)

"""plot area standardized distribution with betobinominal fit"""
plt.figure(figsize=(3.3,2.6),dpi=300)
plt.rc('font', **font) #formatting for plots
plt.plot(size,distribution/area,"ob--",markersize=3)
plt.plot(size,(1-d11_)*betabinom.pmf(x,n_,a_,b_)+d11_,"g-",\
         label=legendt_distribution)
plt.title("betabinominal fitted distribution",size=10)
plt.xlabel('cell size index')
plt.xticks(rotation=45)
```

```
plt.ylabel('Number of cells/area')
plt.legend(loc='best',fontsize='x-small',handlelength=0,
     facecolor='lightgrey')
plt.savefig(graphsfile6)


"""calculate distribution maxima and Full Width Half Maximum"""
r=((1-d11_)*betabinom.pmf(x,n_,a_,b_)+d11_)
peaks, _ = find_peaks(r)
results_half = peak_widths(r, peaks, rel_height=0.5)
results_half[0]  # widths
results_full = peak_widths(r, peaks, rel_height=1)
results_full[0]
halfwidth=results_half[0]
halfwidth_=halfwidth[0]/(numsizes-1) #standardized FWHM
Maxima_x=peaks[0]/(numsizes-1) #standardized x-value of maxima

legendt_dis =  'n={0:d} sizes\na={1:.2f}      b={2:.2f}\nn_B={3:.2f} \
       d={4:.2f}\nFWHM={5:.2f} max_x={6:.2f} \n{7:s}'\
    .format(numsizes,a_,b_,n_,d11_,halfwidth_,Maxima_x,txt)
stream=open(paramsfitfiledis,'w',encoding='utf-8')
stream.write(legendt_dis)
stream.close()

"""plot fitted distribution with maxima and FWHM"""
plt.figure(figsize=(3.3,2.6),dpi=300)
plt.rc('font', **font) #formatting for plots
plt.plot(size,distribution/area,"ob--",markersize=3,label=legendt_dis)
plt.plot(r,"g-")
plt.plot(peaks, r[peaks], "rx")
plt.hlines(*results_half[1:], color="C2")
plt.hlines(*results_full[1:], color="C3")
plt.title("betabinominal fitted distribution",size=10)
plt.xlabel('cell size index')
plt.xticks(rotation=45)
plt.ylabel('Number of cells/area')
plt.legend(loc='best',fontsize='x-small',handlelength=0,
     facecolor='lightgrey')
plt.savefig(graphsfile7)


""""Print Weibull parameters"""
print("Maxima Weibull:","Gen:",numgen,"A1:",A1_,"A2:",A2_,"c:",c_,"tau:",tau_)\
    #parameters weibull maxima fit
print("Minima Weibull:","Gen:",numgen,"A1_m:",A1_m_,"A2_m:",A2_m_,"c_m:",c_m_,\
      "tau_m:",tau_m_)#parameters weibull minima fit

"""print betabinominal parameters"""
print("area:",area)#area under distribution
print("Maxima:",peaks[0]/(numsizes-1),r[peaks[0]])\
    #maxima on standardized cell size index axis
print("halfwidth:",halfwidth_) #halfwidth (FWHM)
print("betabinom:","a:",a_,"b:",b_,"n_B:",n_, "d:",d11_,"maxima_x:",Maxima_x,\
      "FWHM:",halfwidth_)#parameters distribution fit

"""Fitparameters formatting for Table"""
Table = "{0:.5f} {1:.5f} {2:.5f} {3:.5f} {4:.5f} {5:.5f} {6:.5f} {7:.5f} \
 {8:.5f} {9:.5f} {10:.5f} {11:.5f} {12:.5f} {13:.5f}"\
 .format(A1_,A2_,c_,tau_,A1_m_,A2_m_,c_m_,tau_m_,n_,a_,b_,d11_,\
 Maxima_x,halfwidth_).replace(".",",")
stream=open(paramstable,'w',encoding='utf-8')
stream.write(Table)
stream.close()
```

6 Table of Simulation Results

steps	n	m	sigma	alpha	beta	p	gamma	frequency	period	A1_max	A2_max	c_max	tau_max	A1_min	A2_min	c_min	tau_min	n_B	a	b	d	max_x	FWHM
1400000	10	5	1	1	1	1	1,00E-03			673,58877	511,54808	1,01951	162,75981	348,37845	511,54808	0,93297	150,5058	11,27629	1,55522	2,37983	0,01447	0,66667	0,58435
2400000	20	5	1	1	1	1	1,00E-03	0,0422	23,71	663,10941	390,15355	0,78088	1300,45741	216,26646	390,15413	0,95888	2005,49445	29,45129	2,33121	5,90058	0,00225	0,68421	0,54912
3400000	30	5	1	1	1	1	1,00E-03	0,0296	33,82	654,2733	317,44746	0,67325	4382,55354	155,81916	317,44908	0,98197	9734,1435	57,93436	2,9644	11,78308	0,00064	0,68966	0,48987
4400000	40	5	1	1	1	1	1,00E-03	0,0228	43,87	647,97774	269,28181	0,60666	10105,92161	120,70375	269,29368	0,98459	29768,08697	97,52043	3,39699	19,22416	0,00024	0,71795	0,4432
5400000	50	5	1	1	1	1	1,00E-03	0,0186	53,9	643,04949	234,83896	0,56016	18988,09969	98,15331	234,90652	0,98259	70844,01949	147,65016	3,69038	27,50915	0,00011	0,73469	0,4096
6400000	60	5	1	1	1	1	1,00E-03	0,0156	63,92	638,8176	208,90561	0,52576	31433,88203	82,52891	209,01233	0,97933	143899,94359	207,47284	3,89644	36,19425	0,00006	0,74576	0,3846
7400000	70	5	1	1	1	1	1,00E-03	0,0135	73,93	636,82264	188,48459	0,49657	47361,3414	71,10744	188,73195	0,97621	262034,04558	276,2789	4,04719	45,04694	0,00003	0,75362	0,36533
8400000	80	5	1	1	1	1	1,00E-03	0,0119	83,94	636,64292	171,92867	0,47129	66588,97264	62,41135	172,37138	0,97349	440470,47707	353,43077	4,16148	53,93323	0,00002	0,75949	0,3498
9400000	90	5	1	1	1	1	1,00E-03	0,0106	93,95	639,20829	158,08204	0,44748	88254,05891	55,59521	158,85396	0,97172	696529,55075	438,53619	4,25085	62,80178	0,00001	0,76404	0,33712
10400000	100	5	1	1	1	1	1,00E-03	0,0096	103,95	644,8	146,18486	0,42434	111202,16023	50,14785	147,4578	0,97173	1049579,89074	531,03524	4,32335	71,6103	0,00001	0,76768	0,32639
11400000	110	5	1	1	1	1	1,00E-03	0,0088	113,96	652,6343	135,76384	0,40246	134690,69827	45,75547	137,66404	0,97503	1520619,12882	610,29119	4,38199	77,57614	0,00001	0,77064	0,31726
12400000	120	5	1	1	1	1	1,00E-03	0,0081	123,96	660,71185	126,60647	0,38337	159207,48174	42,20494	129,07244	0,98341	2130363,0761	622,10847	4,42467	74,16873	0	0,77311	0,30975
13400000	130	5	1	1	1	1	1,00E-03	0,0075	133,97	669,33412	118,60666	0,36696	184036,9883	39,31201	121,36904	0,99782	2895412,85481	1238,69249	4,42713	141,78197	0	0,77519	0,3053
14400000	140	5	1	1	1	1	1,00E-03	0,0069	143,97	672,82089	111,85744	0,35589	214484,24064	36,89872	114,33659	1,0174	3826133,61479	1342,64636	4,6677	157,49185	0	0,78417	0,28657

steps	n	m	sigma	alpha	beta	p	gamma	frequency	period	A1_max	A2_max	c_max	tau_max	A1_min	A2_min	c_min	tau_min	n_B	a	b	d	max_x	FWHM
5000000	50	1	1	1	1	1	1,00E-03																
5100000	50	2	1	1	1	1	1,00E-03	0,0196	50,98	142,84012	77,05301	0,72131	177756,89156	40,82811	77,14008	0,98904	330663,5228	133,32261	1,70961	8,79879	0,00134	0,77551	0,49691
5200000	50	3	1	1	1	1	1,00E-03	0,0192	51,95	350,27513	138,26994	0,59454	50995,12515	61,6548	138,38051	1,02376	165106,17757	145,92391	2,38989	16,36116	0,00044	0,7551	0,45991
5300000	50	4	1	1	1	1	1,00E-03	0,0189	52,93	531,15991	190,01997	0,55667	26179,92751	80,39374	190,07292	1,0067	102407,23501	150,07197	3,05838	22,87728	0,0002	0,7551	0,43076
5400000	50	5	1	1	1	1	1,00E-03	0,0186	53,9	643,04949	234,83896	0,56016	18988,09969	98,15331	234,90652	0,98259	70844,01949	147,65016	3,69038	27,50915	0,00011	0,73469	0,4096
5500000	50	6	1	1	1	1	1,00E-03	0,0182	54,87	698,39085	274,39865	0,5845	16447,10061	115,28226	274,42308	0,96016	52502,83423	141,85755	4,27501	30,3442	0,00007	0,71429	0,39532
5600000	50	7	1	1	1	1	1,00E-03	0,0179	55,84	721,6623	309,60341	0,61789	15418,16921	131,99416	309,62183	0,94092	40798,01459	134,73997	4,80664	31,75206	0,00005	0,71429	0,38595
5700000	50	8	1	1	1	1	1,00E-03	0,0176	56,8	729,65032	341,22332	0,65499	14897,307	148,40269	341,22421	0,92439	32812,42793	127,27856	5,28129	32,07314	0,00004	0,69388	0,37874
5800000	50	9	1	1	1	1	1,00E-03	0,0173	57,76	731,1647	369,75621	0,69219	14523,21227	164,59976	369,7562	0,91026	27082,46737	119,96124	5,69624	31,59297	0,00003	0,67347	0,37479
5900000	50	10	1	1	1	1	1,00E-03	0,017	58,72	729,78327	395,63871	0,7288	14193,74563	180,58663	395,63788	0,89777	22800,76411	113,00605	6,04959	30,53321	0,00003	0,67347	0,37222
6000000	50	11	1	1	1	1	1,00E-03	0,0168	59,68	727,23449	419,20426	0,76441	13870,15864	196,41767	419,20336	0,88661	19501,52035	106,51101	6,34038	29,06976	0,00003	0,65306	0,37152
6100000	50	12	1	1	1	1	1,00E-03	0,0165	60,63	724,31645	440,72637	0,7989	13539,8433	212,05143	440,72512	0,87619	16885,09274	100,51962	6,5688	27,34487	0,00003	0,65306	0,37188
6200000	50	13	1	1	1	1	1,00E-03	0,0162	61,58	721,37895	460,43221	0,83231	13201,42734	227,4647	460,4313	0,86621	14762,73135	95,03546	6,73594	25,46822	0,00003	0,63265	0,37333
6300000	50	14	1	1	1	1	1,00E-03	0,016	62,53	718,57804	478,51476	0,86473	12855,96253	242,67996	478,51381	0,85658	13010,42278	90,03932	6,84374	23,52283	0,00003	0,63265	0,37573
6400000	50	15	1	1	1	1	1,00E-03	0,0158	63,48	716,00537	495,1379	0,89617	12503,3295	257,66435	495,13729	0,84701	11537,93712	85,51018	6,89516	21,57468	0,00003	0,61224	0,37877
6500000	50	16	1	1	1	1	1,00E-03	0,0155	64,42	713,648	510,44415	0,92682	12146,9367	272,42297	510,44337	0,8375	10284,51065	81,40397	6,89336	19,66541	0,00003	0,61224	0,38282
6600000	50	17	1	1	1	1	1,00E-03	0,0153	65,36	711,52681	524,55626	0,95666	11786,74757	286,95236	524,55576	0,82794	9204,56359	77,70229	6,84295	17,83486	0,00003	0,59184	0,3873
6700000	50	18	1	1	1	1	1,00E-03	0,0151	66,3	709,62018	537,58285	0,98579	11424,31078	301,05459	537,58254	0,81765	8254,89558	74,36729	6,74838	16,10379	0,00004	0,59184	0,39269
6800000	50	19	1	1	1	1	1,00E-03	0,0149	67,23	707,91556	549,61961	1,01425	11060,07093	314,75939	549,61913	0,80673	7414,11007	71,3679	6,61459	14,48683	0,00004	0,57143	0,39864
6900000	50	20	1	1	1	1	1,00E-03	0,0147	68,16	706,39304	560,75037	1,04205	10694,88862	328,35735	560,75023	0,79613	6676,61524	68,67349	6,44664	12,99146	0,00005	0,57143	0,40522
3000000	50	30	1	1	1	1	1,00E-03	0,013	77,18	697,80993	635,63482	1,28654	7133,55599	438,47151	635,63491	0,65409	2145,72631	53,35413	3,91389	4,10145	0,00013	0,46939	0,51325
3000000	50	40	1	1	1	1	1,00E-03			694,95023	670,46444	1,45894	4223,23986	456,33041	670,46454	0,43503	279,55833	49,19227	1,92489	1,6332	0,00021	0,40816	0,69443

steps	n	m	sigma	alpha	beta	p	gamma	frequency	period	A1_max	A2_max	c_max	tau_max	A1_min	A2_min	c_min	tau_min	n_B	a	b	d	max_x	FWHM
5400000	50	5	1	1	1,9	1	1,00E-03	0,0185	53,95	1142,03379	280,27474	0,4496	15607,5878	97,62499	280,89096	0,97711	125789,49125	244,28094	4,23251	65,83473	0,00004	0,77551	0,3382
3000000	50	5	1	1	1,8	1	1,00E-03	0,0185	53,94	1088,73326	276,44167	0,45743	15934,64935	97,71385	276,98699	0,97774	119986,93975	234,32293	4,19662	61,52048	0,00004	0,77551	0,34355
3000000	50	5	1	1	1,7	1	1,00E-03	0,0185	53,94	1035,0248	272,38566	0,46592	16270,73089	97,79869	272,86449	0,97837	114120,62206	224,12781	4,15684	57,18897	0,00004	0,77551	0,34938
3000000	50	5	1	1	1,6	1	1,00E-03	0,0185	53,94	980,63432	268,08153	0,47527	16628,12941	97,88051	268,49768	0,97903	108187,94621	213,75459	4,11259	52,86427	0,00005	0,7551	0,35513
3000000	50	5	1	1	1,5	1	1,00E-03	0,0185	53,93	925,52595	263,4987	0,48569	17010,42161	97,95798	263,85598	0,97971	102183,89637	203,18215	4,06306	48,54767	0,00005	0,7551	0,36167
3000000	50	5	1	1	1,4	1	1,00E-03	0,0185	53,93	869,36839	258,60093	0,49754	17438,71285	98,02867	258,90265	0,9804	96102,31194	192,41112	4,00722	44,24776	0,00006	0,7551	0,36896
3000000	50	5	1	1	1,3	1	1,00E-03	0,0185	53,92	812,63426	253,34237	0,51089	17889,23737	98,08776	253,59306	0,98106	89934,94821	181,49895	3,94396	39,98934	0,00007	0,7551	0,37751
3000000	50	5	1	1	1,2	1	1,00E-03	0,0185	53,92	756,69091	247,66974	0,52501	18260,1194	98,13281	247,87252	0,98169	83675,63763	170,36269	3,87148	35,76125	0,00008	0,73469	0,38695
3000000	50	5	1	1	1,1	1	1,00E-03	0,0186	53,91	700,94251	241,50536	0,54035	18566,98679	98,16069	241,67153	0,98228	77316,25965	159,07563	3,78786	31,59539	0,00009	0,73469	0,39731
5400000	50	5	1	1	1	1	1,00E-03	0,0186	53,9	643,04949	234,83896	0,56016	18988,09969	98,15331	234,90652	0,98259	70844,01949	147,65016	3,69038	27,50915	0,00011	0,73469	0,4096

3000000	50	5	1	1	0,9	1	1,00E-03	0,0186	53,89	587,05392	227,36817	0,5791	19151,33739	98,12024	227,45362	0,98298	64249,65865	136,05411	3,57524	23,51284	0,00013	0,71429	0,42428
3000000	50	5	1	1	0,8	1	1,00E-03	0,0186	53,88	529,71847	219,11368	0,60273	19301,72264	98,02618	219,16973	0,98291	57517,57092	124,36337	3,43761	19,6455	0,00016	0,71429	0,44129
3000000	50	5	1	1	0,7	1	1,00E-03	0,0186	53,86	471,81925	209,7879	0,63035	19325,78835	97,81053	209,84253	0,98188	50609,36286	112,59681	3,27049	15,93744	0,00021	0,71429	0,46135
3000000	50	5	1	1	0,6	1	1,00E-03	0,0186	53,84	413,07223	199,14945	0,66458	19173,85018	97,50249	199,17361	0,98022	43553,80394	100,80977	3,06402	12,43343	0,00027	0,69388	0,4847
3000000	50	5	1	1	0,5	1	1,00E-03	0,0186	53,81	353,45039	186,70579	0,7071	18738,48947	97,00264	186,71393	0,97703	36320,10323	89,10361	2,80412	9,19535	0,00037	0,67347	0,51508
3000000	50	5	1	1	0,4	1	1,00E-03	0,0186	53,76	292,71739	171,74375	0,76166	17858,12368	96,1523	171,74887	0,97069	28897,49941	77,64861	2,47092	6,30765	0,00051	0,65306	0,55602
3000000	50	5	1	1	0,3	1	1,00E-03	0,0186	53,68	230,31633	153,03305	0,83631	16308,66951	94,51816	153,03388	0,95623	21264,97003	66,9232	2,04207	3,90645	0,00071	0,65306	0,61516
3000000	50	5	1	1	0,2	1	1,00E-03	0,0187	53,54	163,40172	128,13707	1,01609	14854,11735	90,96526	128,13706	0,92507	13552,98238	58,82231	1,5289	2,22956	0,00102	0,65306	0,70391

steps	n	m	sigma	alpha	beta	p	gamma	frequency	period	A1_max	A2_max	c_max	tau_max	A1_min	A2_min	c_min	tau_min	n_B	a	b	d	max_x	FWHM
3000000	50	5	0,9	1	1	1	1,00E-03	0,0185	53,91	257,3157	137,15403	0,75974	49295,85243	-13,19752	137,2569	0,63235	33694,17628	213,86534	4,75028	27,89301	0,00227	0,46939	0,48774
3000000	50	5	0,95	1	1	1	1,00E-03	0,0186	53,9	442,50034	187,24388	0,60386	25719,87452	38,77223	187,47401	0,66342	42038,80783	216,56587	4,09108	34,92282	0,00053	0,63265	0,48049
5400000	50	5	1	1	1	1	1,00E-03	0,0186	53,9	643,04949	234,83896	0,56016	18988,09969	98,15331	234,90652	0,98259	70844,01949	147,65016	3,69038	27,50915	0,00011	0,73469	0,4096
3000000	50	5	1,05	1	1	1	1,00E-03	0,0186	53,89	937,51798	279,94022	0,48856	11436,04329	101,1044	280,15373	0,97256	63692,35555	96,11041	3,31783	19,48602	0,00007	0,79592	0,33853
3000000	50	5	1,1	1	1	1	1,00E-03	0,0186	53,89	2187,93228	322,71931	0,32642	1613,46467	109,56781	323,282	1,00269	59669,13251	64,26664	2,93947	13,47905	0,00011	0,83673	0,2847